Advances in Colloid and Interface Science 346 (2025) 103681

Contents lists available at ScienceDirect

Advances in Colloid and Interface Science

journal homepage: www.elsevier.com/locate/cis

Isothermal microcalorimetry for scaffold design and characterization: Assessing bacterial and host cell interactions and physicochemical stability

Carmen Alvarez-Lorenzo *, Angel Concheiro

Departamento de Farmacología, Farmacia y Tecnología Farmacéutica, I+D Farma (GI-1645), Facultad de Farmacia, Instituto de Materiales (iMATUS) and Health Research Institute of Santiago de Compostela (IDIS), Universidade de Santiago de Compostela, 15782 Santiago de Compostela, Spain

ARTICLE INFO

Keywords:
Isothermal microcalorimetry
Interface events
Tissue engineering
Infection
Biofilm
Stability
Cell growth

ABSTRACT

Scaffolds used in regenerative medicine are increasingly expected to address personalization, bioactivity, and sustainability, underscoring the need for characterization methods that reliably predict safety and efficacy. Isothermal microcalorimetry (IMC) offers a highly sensitive, label-free, real-time measurement of heat flow from energy-generating or -consuming process at scaffold interfaces. By monitoring microbial activity, host cell metabolism, material stability, and responses to environmental or therapeutic factors, IMC provides physiologically relevant insight into scaffold performance over extended periods. Its non-destructive, low-preparation, and passive nature preserves samples for complementary analyses, making it a versatile yet underutilized tool in biomedical research. This review introduces IMC for scaffold design and characterization, emphasizing its capacity to evaluate vulnerability to biofilm formation and the effectiveness of anti-biofilm strategies. It further explores applications in tracking scaffold formation, assessing host cell-material interactions and tissue development, and probing the antitumor potential of engineered scaffolds. The review concludes with a perspective on IMC's role in advancing scaffold translation within the evolving regulatory landscape shaped by the FDA Modernization Acts 2.0 and 3.0.

1. Introduction. Design of scaffolds in the 21st century

Scaffolds for regenerative medicine are no longer merely passive materials serving as physical supports for cell growth. In the context of the Fifth Industrial Revolution (Industry 5.0), scaffolds—like all modern medical devices—are now expected to meet demands for personalization, bioactivity, and sustainability [1].

Throughout the 20th century, industries developed efficient mass production techniques and protocols, leading to cost reductions and continuous improvements in product quality. Automation made a wide range of products, including those related to health and welfare, more accessible to broader populations. However, by the early 21st century, not only affordability but also enhanced performance and personalization is increasingly demanded. As a result, the paradigm shifted from mass production to mass personalization or customization, with many new associated challenges [2].

Driven by next-generation information technologies, Industry 5.0 emphasizes "personalization," placing human well-being at the core of manufacturing systems [3]. It builds upon the technological advancements of Industry 4.0 by offering highly personalized products and services, empowering consumers to play an active role in product development. The defining features of Industry 5.0 are human-centricity, sustainability, and resilience. In healthcare, digitalization has transformed patient care through earlier diagnosis, faster development of targeted treatments, and more integrated data and monitoring systems, all with reduced manual effort [4]. Industry 5.0's focus on personalized automation has made the individualized delivery of care a reality. Personalized medicines, patient-specific implants, artificial organs, custom transplants, and individualized surgical planning and instruments are now increasingly feasible [5,6].

Beyond personalization, 21st-century research on medical devices must also address two critical challenges: eco-sustainability and antimicrobial resistance. Scaffolds tailored to individual patient needs require novel fabrication technologies and bioactive (cell-instructing) materials that strike a balance among safety, cost, sustainability, and environmental impact [7–9]. Growing concerns over plastic waste from medical device production and use are prompting researchers to seek biodegradable and eco-friendly alternatives to synthetic polymers—often turning to terrestrial and marine biological or bioinspired sources [10–12]. Additionally, improving the physicochemical stability

* Corresponding author.
E-mail address: carmen.alvarez.lorenzo@usc.es (C. Alvarez-Lorenzo).

https://doi.org/10.1016/j.cis.2025.103681
Received in revised form 25 August 2025;
Available online 29 September 2025

of current materials to extend their shelf life is a key area of interest [13].

In the era of antimicrobial resistance, tissue regeneration faces two major challenges: many wounds and damaged tissues are already infected before treatment, and scaffold implantation carries inherent infection risks, especially from nosocomial bacteria introduced during surgery. Biofilm formation is notoriously difficult to eliminate, making prevention crucial. To develop materials that can resist or combat bacterial colonization, better techniques are needed to characterize scaffold-bacteria interactions. As noted by Serrano-Aroca et al. (2022), the design of infection-resistant scaffolds requires attention to fabrication, material properties, and bioactivity [14]. Assessing bacterial viability is essential to evaluate infection risks and avoid cross-contamination of tissues and patients, ensuring public health. Traditional methods rely on three main indicators: culturability, membrane integrity, and metabolic activity. While culture-based techniques assess the ability of bacteria to grow on media, they fail to detect viable but non-culturable cells, i.e., living microorganisms that have lost their ability to grow and reproduce on standard laboratory media but remain metabolically active and capable of resuming growth under different conditions. Membrane integrity assays, though more comprehensive, are often complex and equipment-intensive. Metabolic activity-based methods can detect non-culturable cells but may still miss dormant bacteria that temporarily cease metabolic function [15].

Similar to bacterial assessments, the evaluation of mammalian cell compatibility with scaffolds and tissue growth is typically done at fixed time points. These endpoint measurements offer a static snapshot but often miss dynamic interactions occurring during incubation. Additionally, the impact of pre-treatments—such as sterilization—on scaffold performance, cell/bacteria interactions and short-term biomaterial behavior is frequently overlooked, potentially biasing quality assessments [16,17]. Techniques capable of real-time monitoring of bacterial or cellular activity on scaffolds can provide deeper insights into these interactions, aiding the rational design of next-generation scaffolds.

In this context, isothermal microcalorimetry (IMC)—an established yet still underutilized technique—is attracting renewed interest. One of its main advantages is the ability to analyze virtually any type of material, from liquids to solids, without extensive preparation. Biomaterials and scaffold samples can be directly placed into microcalorimeter ampoules. By continuously monitoring heat flow in comparison to controls, IMC enables the quantification of both physical degradation processes (such as hydrolysis or corrosion) and biological interactions, including the adhesion of mammalian cells or bacteria to material surfaces, in terms of both rate and magnitude [18,19].

This review first introduces IMC, highlighting its advantages and limitations for biomedical applications, with a particular focus on monitoring events at biomaterial–biological interfaces. The literature to date has primarily focused on using IMC to monitor microbial growth. Accordingly, the subsequent sections of this review will analyze the heat flow signatures of bacterial and fungal activity and assess IMC's potential to evaluate scaffold susceptibility to biofilm formation and the effectiveness of anti-biofilm additives. Finally, the review will explore IMC applications in monitoring the formation and physicochemical stability of scaffold-forming biomaterials, evaluating mammalian tissue development, and assessing the antitumoral activity of implanted scaffolds.

2. Direct microcalorimetry

Every living organism is in constant heat exchange with its environment. All metabolic processes that occur within an organism produce heat and every living organism is an open system that constantly exchanges heat with its surroundings. Heat production occurs via cellular metabolism (bioenergetics) and cell work. Measuring the heat released requires a very sensitive system—the calorimeter.

Calorimetry derives from the Latin word 'calor' (heat) and the Greek word 'metrion' (measure). Direct calorimetry is the gold standard means of quantifying the heat produced from aerobic and anaerobic metabolism by measuring heat exchange between the body and the environment [20]. First direct calorimetry systems dated back to the 18th century with the ice calorimeter of Lavoisier and Laplace, who pioneered the measurement of animal heat and demonstrated that it mainly comes from the combustion of carbon-based sources (Fig. 1A) [21]. In the late 19th century, the first human calorimeters were constructed. The Atwater–Rosa calorimeter, also known as a respiration calorimeter, was the most popular since it was able to integrate indirect and direct calorimetric measurements, although it required more than 6 h for the measurements to stabilize (Fig. 1B). This calorimeter enabled the measurement of gaseous exchange between a living organism and the surrounding atmosphere (indirect calorimetry), as well as the simultaneous measurement of the heat produced by that organism (direct calorimetry) (Fig. 1C) [22].

The calorimeters evolved in the last 200 years, and today whole-body human metabolism is measured using indirect calorimetry, while direct calorimetry is reserved for cell-scale measurements. Direct calorimetry relies on the fact that the heat of a reaction can be measured as the heat flux or exchanged between a substance and its environment, if the reaction occurs in an enclosed, isolated system of known heat capacity. The reaction heat (heat energy) is quantified by the change in temperature of the system. By definition, heat is the quantity of energy exchanged per unit time between two systems in the form of a heat exchange. Thus, calorimetry is the measurement of heat energy, and a calorimeter is used to measure this heat. To be effective, a calorimeter must be a closed system to ensure that all of the produced heat is measured, and no transfer of energy occurs between the calorimeter and its surroundings. Unlike indirect calorimetry, direct calorimetry measures the total heat dissipated by the body because of both anaerobic and aerobic metabolisms [20]. Assessing the rate of oxygen consumption provides insight into the level of aerobic respiration. When heat dissipation and oxygen consumption are measured together, the calorespirometric ratio can be calculated, revealing the relative contributions of aerobic and anaerobic respiration [23].

Traditional direct calorimeters measure heat released from the cells using either air or water to absorb and carry away the heat. This method relies on the specific heat capacity of the chosen medium, i.e. the amount of heat needed to raise its temperature by 1 °C. By measuring the temperature change of the medium and knowing its specific heat capacity, the amount of heat exchanged can be calculated.

Differently to other calorimeters, isothermal microcalorimeters (IMCs) can measure heat production rates as low as a microwatt (μW = μJ/s) and operate at nearly constant temperature. This allows for continuous and highly accurate monitoring of the metabolism and growth of small populations of cultured bacteria, protozoa, human cells, and even small animals at any chosen temperature. In IMCs, heat generated or absorbed within the calorimetric ampoule flows to or from a heat sink, typically an aluminum block. This process helps maintain the ampoule and its contents within a few millidegrees of the heat sink's temperature, which is regulated by the calorimeter's thermostatic system. The actual sensors in this setup are thermoelectric modules, such as Seebeck or Peltier modules, positioned between the sample and the heat sink. These modules detect even the slightest temperature differences and convert them into electrical signals, which can then be easily recorded [19].

The development of microcalorimeters with multichannels, also known as multicalorimeters (Fig. 1D), opens the possibility of evaluating several specimens or samples of the same specimen as well as controls in the same run [24]. Microcalorimeters adapted to 48-well microtiter plate have recently been designed [25]. Flow microcalorimeters are being also developed to monitor cell growth in bioreactors intended for biotechnological production of biopharmaceuticals [26].

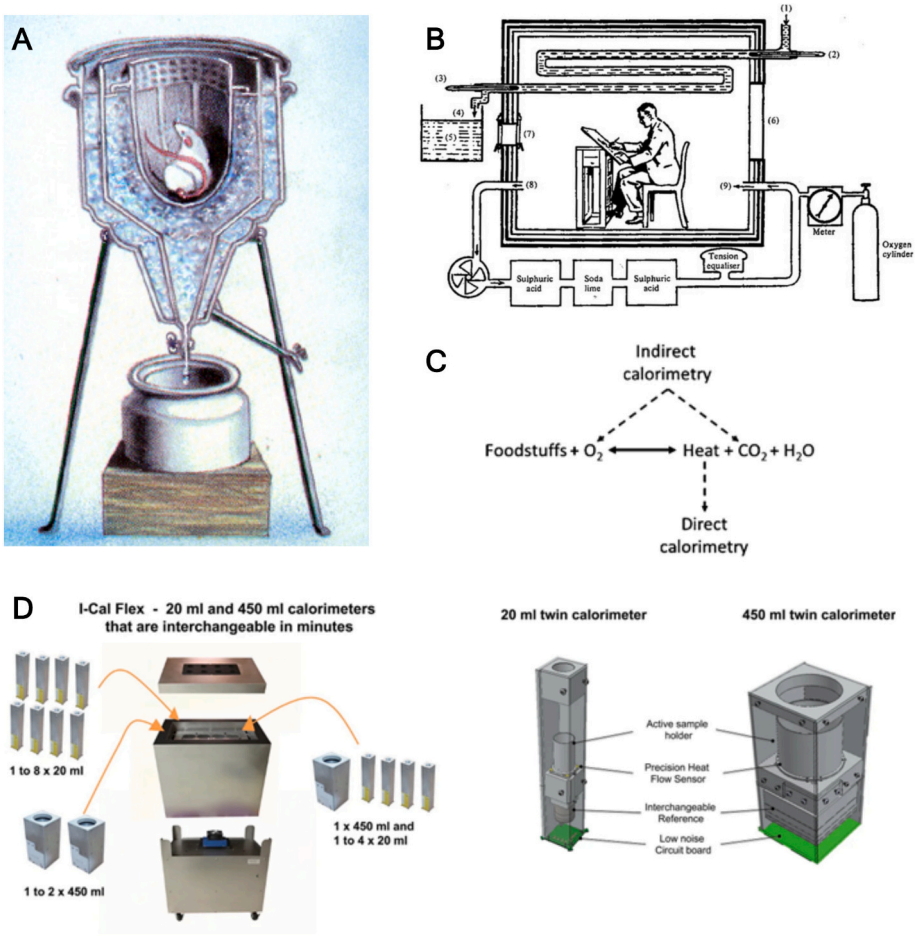

Fig. 1. (A) A cross-sectional view of the ice calorimeter developed by Lavoisier and Laplace. An animal is placed in the inner chamber, and ice is placed in the outer chamber. Heat produced by the animal can be measured indirectly by assessing the amount of water (from ice melting) that elutes from the bottom of the chamber, which is the impact of the animal's heat on the ice in the outer chamber. Reproduced from Da Poian et al. [21]. (B) The Atwater and Benedict's calorimeter; numbers 1–5 represent the direct calorimetry portion of the chamber. Water flows through the system from 1 to 4 and is collected in a reservoir at 5. Thermometers are placed at 2 and 3 to determine changes in water temperature between the inlet and outlet. The subject enters/exits the chamber via number 6 (door), whilst 7 represents a glass window. The closed-circuit respirometer is represented by 8 and 9. The air in the chamber is collected through 8, enters the system and undergoes oxygen replacement before returning to the chamber through 9. Reproduced from Archiza et al. [22] with permission of Springer Nature. (C) While direct calorimetry measures the actual heat generated by biological processes, indirect calorimetry estimates heat production by assessing the rate of oxygen (O_2) consumption and carbon dioxide (CO_2) production during metabolic activity, whether at rest or during physical exertion. Reproduced from Kenny et al. [20] with permission of Springer Nature. (D) Scheme of the I-Cal Flex isothermal microcalorimeter, which can accommodate up to 8 sample cells of 20 mL each, 2 larger cells of 450 mL, or a hybrid setup with 4 smaller (20 mL) cells and 1 larger (450 mL) cell tested simultaneously. Each twin calorimeter cell is individually calibrated using fixed internal calibration heaters. To ensure precision and stability, the cells are isolated by a wide air gap, which eliminates thermal interference (crosstalk) between them. A high-precision thermostat maintains temperatures between 2 °C and 90 °C, with a stability of ±0.001 °C over extended periods. This allows for long-term experiments lasting weeks or even months without temperature fluctuations affecting results. Reproduced from [24].

2.1. Advantages and limitations of direct microcalorimetry

Microcalorimetry is particularly useful for studying how environmental changes or added substances affect microorganisms and mammalian cells survival or cell-scaffold interactions over periods ranging from hours to days. It is a non-destructive technique that requires minimal sample preparation and is entirely passive, preserving the sample for further analysis [19,27]. Main general advantages and limitations of direct microcalorimetry are listed below.

Main advantages refer to:

- Versatility: Dynamic measurements of virtually any chemical or physical process by recording related heat production or consumption.
- Sensitivity: Most microcalorimeters have a sensitivity of at least 2 μW or lower. Thus, only small specimens (e.g., g or mL range and smaller) are required. Considering that one active mammalian cell generates between 1 and 100 pW [28,29], samples containing a relatively small number of cells, e.g. 10^4–10^5, generate quantifiable results.
- Accuracy: Commercially available microcalorimeters have high temperature stability (0.001 °C) and very small baseline drift (< 5 μW in 24 h).
- Continuous real-time data: Microcalorimeters report real-time electronic signals proportional to the heat production rate. Typical sampling is 1 data point per second or per minute, depending on the length of the test.
- Non-destructive, passive technique: The sample requires no pretreatment (no fluorescent- or radio-labeling), remains unmodified, and is not altered during measurement. Typically, it is placed in sterile vials with either air or a specific gas mixture in the headspace to simulate aerobic or anaerobic conditions, ensuring a stable environment over time. For instance, 20-mL vials containing mammalian cells cultured in 3 mL of medium can hold enough air in the

headspace to support growth conditions comparable to those in 6- and 12-well plates. Additionally, the sample remains suitable for further analysis using other techniques after microcalorimetric measurements.
- Only produced heat is measured, therefore changes in pH, turbidity, viscosity… do not significantly interfere in the measurement.

The main limitations of IMC, along with strategies to overcome them, are listed below.

- Non-specific signal. Heat can be generated from multiple sources, necessitating careful experimental design. For instance, controls without cells or scaffolds are essential to distinguish heat flow specifically associated with cell growth from other potential sources, such as medium or scaffold degradation or unintended contamination. Readers seeking further details on methods developed for studying mammalian cell processes are encouraged to consult a comprehensive review [27]. Growth of microbiota in human tissue biopsies can be prevented by culturing with antibiotics [30].
- Variables such as sample volume, medium composition, oxygen availability, and temperature can strongly influence cellular metabolic activity and the resulting heat flow signals [31,32]. To ensure comparability of results, experimental conditions should therefore be reported in full detail. For example, different medium volumes alter the ratio of culture medium to headspace air in capped vials. In aerophilic microbial strains using 20 mL IMC vials, the strongest thermal power output and highest cell growth were observed with 3–6 mL cultures. Increasing the medium volume to 12 mL caused a marked decrease in IMC signals due to oxygen restriction [33]. As a general guideline, the sample should occupy no more than one-fourth of the vial volume to avoid oxygen-dependent artifacts, yet not be so small relative to vessel size that reliable signals cannot be obtained.
- Extended stabilization time. Accurate heat flow measurements require that the sample vial equilibrates to the exact temperature of the microcalorimeter. This stabilization process can take up to an hour before the recorded signal reliably reflects the biological or chemical activity inside the vial. Preheating the vials and culture medium to the test temperature can help reduce the stabilization time.
- Lack of cell identification. IMC does not inherently distinguish which cells are growing within the vial (e.g., in mixtures of bacterial and/or human cells). This limitation can be addressed by combining IMC with complementary techniques once the vial is removed from the instrument. Advanced microcalorimeters equipped with additional sensors for physicochemical properties or biomarkers can also provide complementary information during the measurement [34]. Furthermore, the growth of specific target microorganisms can be selectively promoted by using tailored culture media that suppress competing organisms [35].

The distinct and significant advantages of the IMC make it potentially useful for numerous applications in biomedicine, yet it remains underexplored [19,36,37]. Curiously, IMC is still relatively unknown in the biological field, likely due to the limited emphasis on bioenergetics and biothermodynamics in the curricula of most biomedical-related undergraduate programs [38]. Moreover, IMC is frequently overshadowed by more widely adopted calorimetric techniques, such as titration calorimetry (ITC) and differential scanning calorimetry (DSC), which are primarily employed to characterize (bio)molecular interactions or temperature-induced transitions, respectively [39–41]. Nonetheless, IMC is particularly well-suited for measuring the metabolic activity of animal cells. The heat flux produced by cells growing in vitro offers a direct measure of their specific metabolic activity, as the majority of the substrate's Gibbs free energy is dissipated as heat, with only a small portion retained as entropy within newly synthesized biomass [42]. Overall, IMC provides both kinetic and thermodynamic information of the process being evaluated [43].

The following sections highlight key applications of IMC, including its use in detecting infections, assessing the effectiveness of scaffolds loaded or coated with antimicrobial agents, monitoring cell growth for tissue engineering, evaluating the stability and biocompatibility of materials used in medical and surgical devices, and investigating the potential of drug-eluting implantable scaffolds to control tumor growth.

3. IMC for bacteria growth and infection models

Microcalorimetry has been widely used to monitor microbial activity [44,45], largely due to the rapid growth of microorganisms and the significant heat they generate. However, the signals must be carefully interpreted and ideally compared to other methods contrasted in microbiology in order to validate the use of IMC for each bacteria [38].

Among the non-calorimetric techniques, culture in appropriate medium and plate counting remains as the golden standard. This technique is time consuming, requiring several days to obtain reliable results. As an alternative, spectrophotometric methods can enable monitoring of cell growth, but they cannot differentiate between turbidity caused by viable cells and that caused by dead cells. Modern methods based on metabolic and biochemical assays are gaining increasing interest [46]. While gene-based methods can provide rapid microbial detection, they have limitations. Many of these methods do not distinguish between live and dead microorganisms (i.e., those actively replicating or metabolizing). Additionally, genetic identification of antibiotic resistance is limited to microorganisms with already known resistance-related genes.

Together with the unique features mentioned in section 2, IMC is notably advantageous for detecting viable but non-culturable cells and analyzing turbid or solid samples. Unlike most methods, which struggle to identify anaerobic bacteria due to their strict growth requirements, IMC enables faster and simpler detection by reducing the air volume in the vials, simply adding more culture medium [47]. Additionally, since most bacteria grow rapidly, the minimum cell density for heat flow quantification -usually in the 10^4–10^5 range- can be reached rapidly even starting from samples with very low bacteria contamination [46]. Linear relationships between calorimetric detection time and initial bacterial concentrations have been found for growth in both liquid and solid media. Such relationships can be used to directly quantify bacterial contamination in a variety of products and as an aid in membrane filtration protocols for sterility control of pharmaceutical products since IMC measurements are significantly faster than visual inspection [32,48]. However, direct translation of heat flow curves into biologically relevant information, such as growth rate (μ) and the generation time (g) is not straightforward [49].

Typical heat flow curves of bacteria growth are collected in Fig. 2 [49]. The thermograms show a rise and fall pattern as also occurs when microbial growth in batch culture is recorded (Fig. 2A). However, the patterns may be quite different as they record different properties. Microbial growth commonly follows four phases: lag, exponential, stationary, and death. IMC patterns are usually more complex and a decrease in heat flow does not always indicate a drop in cell number (Fig. 2B). Interestingly, IMC can sometimes detect two or more peaks when microorganisms exhibit a bi-phasic growth pattern. This occurs because multiple carbon sources are metabolized sequentially. The microorganisms first consume one food source, then switch to another, which causes a temporary drop in heat flow while the new enzymes required are being synthesized (e.g., β-galactosidase under catabolite repression; Fig. 2C) [50]. Such double peaks in heat flow curves can also be seen in complex environments like milk or sourdough fermentation. Likewise, metabolic shifts—such as switching from aerobic respiration to fermentation—can cause transient decreases in heat flow (Fig. 2D) [34].

Importantly, the return of heat flow to baseline does not imply that cells are dead or absent; rather, it typically means that metabolic activity

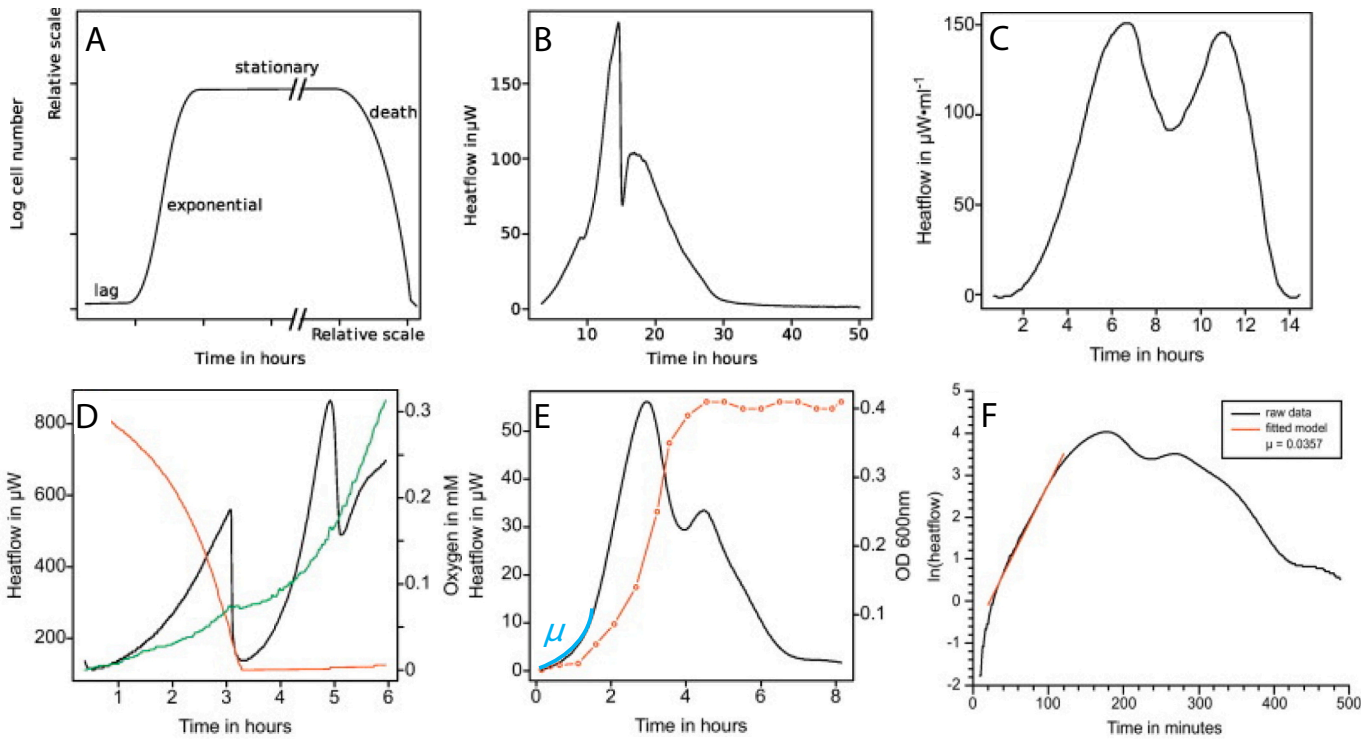

Fig. 2. (A) A typical microbial growth curve and (B) microcalorimetric pattern of *Enterococcus faecalis*. Reproduced from Braissant et al. [49] with permission of Elsevier. (C) Microcalorimetric profile of *Saccharomyces cerevisiae* during sequential utilization of fructose and maltose. Reproduced from Schaarschmidt and Lamprecht [50] with permission of Elsevier. (D) Microcalorimetric pattern of *Escherichia coli* recorded when a decrease in oxygen occurred (indicated by the red curve), which caused a switch from respiration to fermentation (when oxygen is absent). The green line represents the optical density of the culture suggesting an increase in the cell number. Adapted from Johansson and Wadsö [34] with permission of Elsevier. (E) Microcalorimetric pattern of *Escherichia coli* (in black) also showing the increase in cell number measured by optical density (in red); the line in blue represents the portion of exponential growth (μ). Reproduced from Fan et al. [51] under Creative Commons Attribution 4.0 International License. (F) Natural logarithm plot of data reported in plot E can be used to calculate the growth rate (μ). Reproduced from Braissant et al. [49] with permission of Elsevier. (For interpretation of the references to colour in this figure legend, the reader is referred to the web version of this article.)

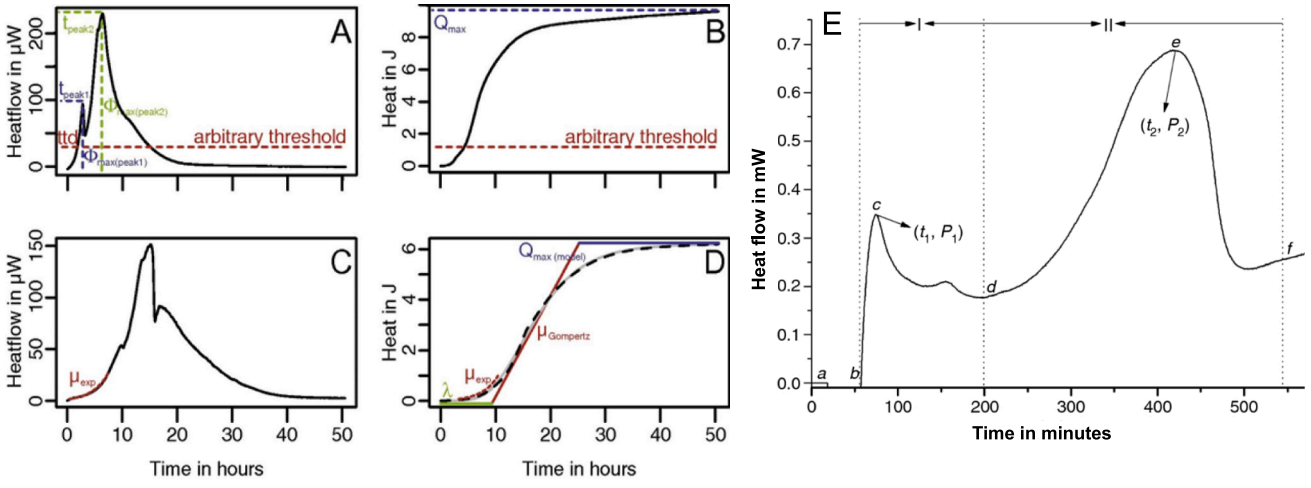

Fig. 3. Typical IMC thermograms of bacteria cultures showing the regions used for the analysis. (A and B) The thermal power curve and corresponding integrated heat measured during *E. coli* growth in Basal Medium Eagle (BME) medium. The time to peak (t_i) and peak height (ϕ_i) are marked. The first intersection of an arbitrary threshold with the thermal power or heat curves can be used to determine the time to detection. Additionally, the maximum heat (Q_{max}) is recorded. (C and D) The thermal power curve and corresponding integrated heat observed during *E. faecalis* growth in BME medium. The growth rate (μ) can be determined from both the thermal power and integrated heat curves. The Gompertz model enables the calculation of the growth rate ($\mu_{Gompertz}$), as well as the lag phase duration (λ) and total heat (Q_{max}). Reproduced from Braissant et al. [38] with permission of Elsevier. (E) The heat flow power–time curve of *S. aureus* growth in Luria–Bertani (LB) medium at 37 °C showing two exponential growth phases (b-c, and d-e); the growth rate constants (k) of the first and second exponential phase can be calculated from the natural logarithm plot of heat flow versus time. Reproduced from Pu et al. [53] with permission of Springer Nature.

has ceased, while viable cells may still be present (Fig. 2E). For example, *E. coli* can survive for days after growth stops, even though heat production ends after about 10 h [51]. Therefore, heat flow reflects cell activity and correlates well with cell number or optical density during early growth, but this relationship breaks down during later phases or under stress. Optical density may continue to rise even as heat flow declines as dead microorganisms also contribute to turbidity. Optical density measurements can be also influenced by a wide number of variables (e.g., pH, temperature, and water activity) [52].

Interpreting calorimetric data requires careful correlation with microbiological measurements—such as colony-forming units (CFU), direct microscopy, or previously validated data—to draw accurate conclusions about microbial viability and growth dynamics. Nevertheless, some useful information can also be directly extracted from the IMC curves mainly when they are used for comparative purposes, such as to evaluate the effect of a certain variable. Braissant and coworkers have proposed various mathematical models to calculate the growth rate (μ), lag phase duration and maximum growth, as explained elsewhere [38,49]. In brief, information on growth onset, time to peak, peak height, time to detection, and time to return to baseline can be easily obtained from the IMC curve (Fig. 3). Simple exponential models allow calculating μ form the early rising portions of the heat flow curve (Fig. 2F; Fig. 3C) or from the heat data considered as the integral of the heat flow over time (Fig. 3B).

When the heat flow curve is allowed to return to values close to the baseline, the accumulated heat (integral) over time curve usually adopts a sigmoid shape. The overall analysis of the S-shaped curve requires using more complex models, such as the logistic, the Gompertz or the Richards growth models that can be applied to the accumulated heat over time curves [49]. Under certain assumptions, these models provide the values of the maximum growth rate (μ_m), the lag phase duration (λ), and the total heat (Fig. 3D). Multiple peaks can be recorded during the experiment, as it is the case of *S. aureus* showing bimodal heat flow power–time curve (stages I and II) with five distinct phases: (i) lag phase (a–b), (ii) first exponential growth phase (b–c), (iii) transition phase (c–d), (iv) second exponential growth phase (d–e) and (v) decline phase (e–f) (Fig. 3E) [53].

Using a similar mathematical framework, kinetic analysis of IMC data has been optimized to monitor the growth of probiotics in the food industry. Notably, by analyzing IMC-derived growth parameters, such as the rate constant and doubling time, the quality of commercial probiotic products could be evaluated within just 15 h, compared to the over one week typically required by conventional plating methods. This highlights the potential of IMC as a powerful tool in industrial quality control, enabling significantly faster product release to the market [54].

In the biomedical field, microcalorimetry has proven to be a powerful tool for quickly detecting infections and microbial contamination in clinical samples and products. For example, bacterial contamination in platelet samples can be detected within a few hours using IMC [55]. Similarly, methicillin-resistant *Staphylococcus aureus* (MRSA) can be rapidly identified and distinguished from susceptible species in less than one day [56,57]. The technique is also effective for detecting slow-growing bacteria, such as *Mycobacterium tuberculosis*, which can be identified within hours to a few days—a major improvement over traditional culture methods that can take up to 60 days [58].

IMC has also been proposed as a tool for early detection of septic arthritis in patients requiring hip and knee prosthesis, aiming to prevent infection-related complications. Low-grade infections are often difficult to distinguish from aseptic mechanical failure, yet they pose a significant risk of developing into prosthetic joint infections (PJI). Biofilm formation not only shortens the lifespan of the prosthesis but also causes inflammation and pain for the patients. Pre-operative analysis of synovial fluid typically involves leukocyte counting, where elevated levels may indicate an infection but do not reveal the underlying pathogen. As an alternative approach, IMC of synovial fluid aspirates from patients with acute arthritis has demonstrated the feasibility of detecting septic arthritis in few hours (less than 9 h depending on the pathogen) [59], which is significantly faster than using conventional culture methodologies (median time 3 days). Compared to multiplex Polymerase Chain Reaction (PCR), which enables detection faster than traditional cultures, IMC proved superior, as PCR failed to detect several microorganisms [60].

In a relevant prospective study involving 107 patients, IMC and synovial fluid culture results were concordant in 98 cases (92 %) (Fig. 4 A). IMC failed to detect infection in 4 patients whose cultures yielded bacterial growth, while conventional cultures missed infections in 4 patients that were identified by IMC. Overall, the two methods showed a high degree of concordance. However, IMC offers the advantage of significantly faster diagnosis, which facilitates earlier antimicrobial treatment and may contribute to shorter hospital stays and reduced healthcare costs [61]. IMC also allows rapid detection of infection in necrotizing fasciitis after breast augmentation [62].

In this line, IMC has also been shown to reduce the time required for diagnosing fracture-related infections without compromising diagnostic accuracy parameters [63]. Proper treatment of fracture-associated infections is critical prior to surgical repair. However, conventional tissue cultures are associated with a 10 % to 20 % false-negative rate, which can compromise the success of subsequent interventions. In a study involving 93 patients with suspected fracture-related infections, the diagnostic speed and accuracy of IMC were compared with conventional cultures. Tissue samples from each patient were homogenized and cultured for aerobic, anaerobic, acid-fast bacilli, and fungal organisms. In parallel, aliquots of the homogenates were placed in growth media and analyzed using a CalScreener® (Symcel) microcalorimeter for a minimum of 24 h. Aerobic and anaerobic cultures were maintained for 5 days and 14 days, respectively. No significant differences were found between IMC and conventional cultures regarding sensitivity, specificity, positive predictive value, negative predictive value, or overall accuracy. The concordance between IMC and conventional culture results was 85 %. However, IMC demonstrated a substantially shorter median time to diagnosis (2 h, range 0.5 to 60 h) compared with conventional cultures (51 h, range 18 to 147 h). Thus, IMC emerges as a rapid and reliable technique for early infection detection, enabling timely initiation of antibiotic therapy while awaiting definitive species identification and susceptibility results from conventional microbiological methods.

IMC is particularly well fitted to predict the risk of tissue grafts to develop biofilms. A comparative study between bone patellar tendon bone (BPTB) grafts and quadrupled hamstring anterior cruciate ligament (4xHt) grafts was carried out to predict infections after the anterior cruciate ligament reconstruction (r-ACL) surgery [64]. Although infections after r-ACL are not as common as other implant-associated infections, this complication can strongly compromise joint function. Therefore, prophylaxis techniques such as bathing the grafts in antibiotic solutions before implantation are commonly applied. In most cases the source of microorganisms is the normal microbiota of the skin, and higher infection rates have been reported after 4xHt autografts surgeries which require sutures [65]. To gain an insight into this issue, the BPTB and 4xHT grafts from biobanks were incubated with a strain of *S. epidermidis* at 37 °C for 24 h, and then washed to remove planktonic cells and placed in a microcalorimeter or sonicated and plated. Since the risk of developing healthcare-related infections depends on surpassing a minimal infective dose (MID), the grafts were exposed to 1×10^5 CFU/mL *S. epidermidis* culture. Both grafts performed similarly in terms of bacterial growth profiles through IMC and CFU counting. Biofilm was observed the same in BPTB and 4xHT grafts, therefore, discarding that the source of the graft can increase the risk of infection.

Bone graft infections have been reported in up to 12 % of surgical interventions. However, the infection risk associated with autologous and allogenic human grafts, as well as bovine cancellous bone grafts, has not been thoroughly quantified through statistical analysis. To address this gap, a comparative study was conducted using various

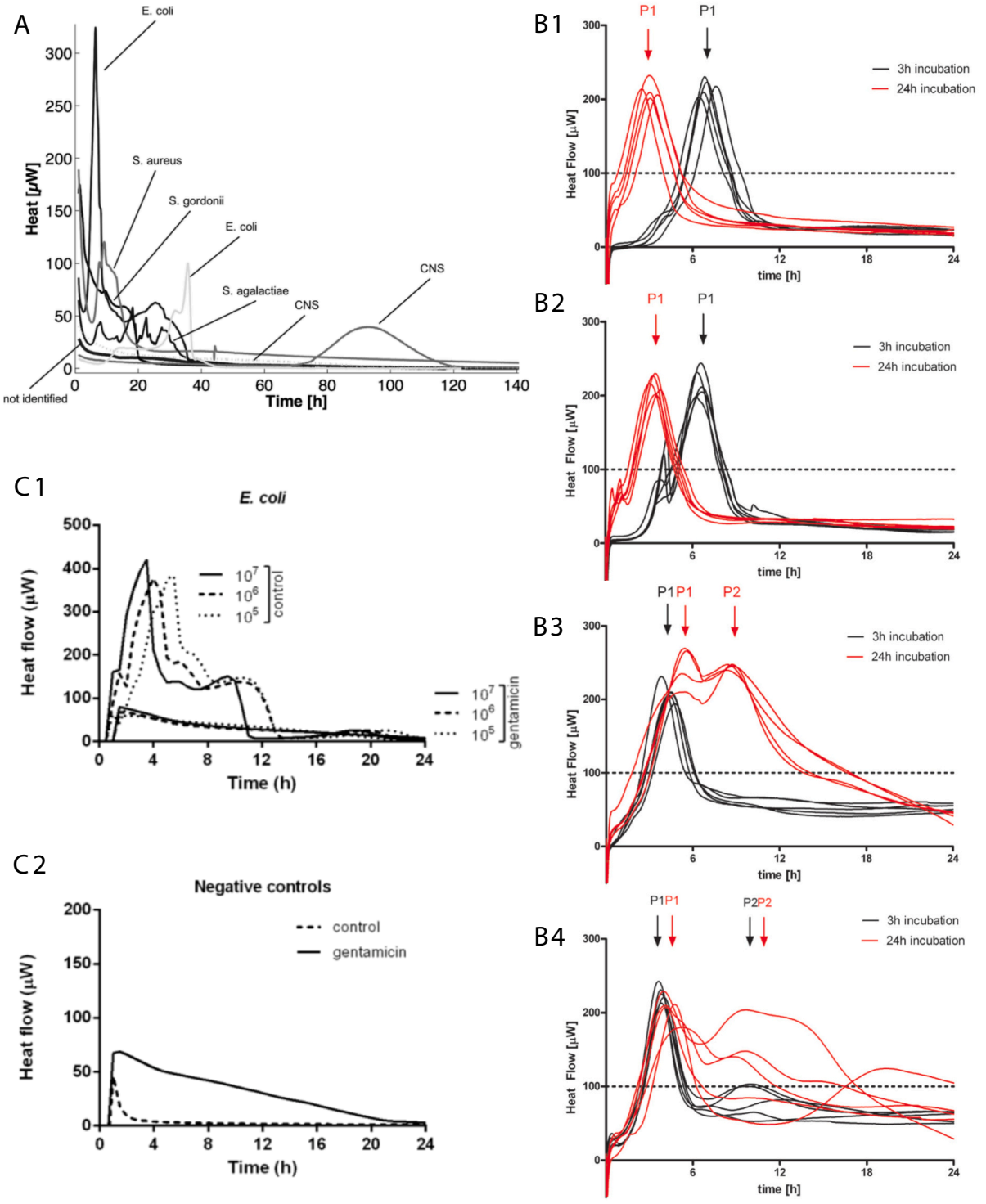

Fig. 4. (A) IMC curves recorded for synovial fluid of patients with periprosthetic joint infection incubated in tryptic soy broth at 37 °C. The microorganisms indicated in the legend were identified in the cultures. CNS refers to coagulase-negative staphylococci. Reproduced from Morgenstern et al. [61] under Creative Commons Attribution 4.0 International License. (B) IMC curves of (B1) processed cancellous human bone grafts (Tutoplast™), (B2) bovine bone grafts (Tutobone™), (B3) fresh human femoral head grafts, and (B4) fresh-frozen human femoral head grafts after being incubated for 3 h or 24 h with *S. aureus* in tryptic soy broth. P1 and P2 correspond to peaks 1 and 2 calculated from all curves. The curves display an initial thermal equilibration phase (negative values within the first 15 min) followed by an exponential rise, reflecting bacterial growth. Once nutrients in the ampoules are depleted, the signal declines with a negative slope. Reprinted from Clauss et al. [66] under Creative Commons Attribution license. (C) IMC results obtained for (C1) *E. coli* at three different densities (10^5, 10^6, and 10^7 CFU/mL) incubated in Müller-Hinton broth with calcium sulfate beads loaded with gentamicin or without drug (control), and (C2) the same beads in growth medium without bacteria at 37 °C. Reprinted from Thein et al. [78] under Creative Commons Attribution license.

commercially available and clinically relevant bone graft types: processed cancellous human bone grafts (Tutoplast™) (Fig. 4 B1), bovine bone grafts (Tutobone™) (Fig. 4 B2), and both fresh (Fig. 4 B3) and fresh-frozen (Fig. 4 B4) human femoral head grafts [66]. Samples were incubated with 1×10^5 CFU/mL *S. aureus* in tryptic soy broth (TSB) for either 3 h or 24 h to generate early biofilm and mature biofilm, respectively. Following incubation, the grafts were washed and sonicated, and the sonication fluid was used for CFU quantification. The sonicated grafts were placed in ampoules with 1 mL of medium and the heat flow was recorded using a TAM III calorimeter (TA Instruments, New Castle, DE, USA). In this case, the calorimetric time to detection (TTD) was defined as the time from ampoule insertion to the onset of an exponentially increasing heat-flow signal exceeding 100 μW. This threshold was chosen to ensure that only metabolically active, replicating bacteria were measured. Processed human and bovine bone grafts exhibited a single heat flow peak, with shorter TTDs for mature biofilm, consistent with the higher CFUs recorded. In contrast, fresh human grafts showed two distinct peaks across all conditions, with similar TTDs for 3 h and 24 h incubation (Fig. 4 B3); however, the second peak was more pronounced for the mature biofilm. Fresh-frozen bone grafts displayed a single peak after early biofilm formation (3 h) and two peaks following mature biofilm incubation (24 h) (Fig. 4 B4).

The different behavior observed can be related to the fact that fresh and fresh frozen human grafts retain serum proteins and residual bone marrow; features completely absent in the commercially processed grafts. After incubation with fresh human grafts (3 and 24 h) and fresh frozen human grafts (24 h), a subpopulation of *S. aureus* small colony variants (SCVs) was observed alongside normal-sized colonies. SCV, which are approximately one-tenth the size of conventional colonies, represent a slow-growing, metabolically altered phenotype known for enhanced persistence and resistance to treatments. The second peak observed in the heat flow curves likely corresponds to the metabolic activity of these SCVs, which utilize the proteins present in fresh grafts as alternative energy sources not provided by standard TSB medium [66]. This finding underscores the importance of using biorelevant media when assessing the potential of bone grafts to support SCV formation and biofilm development. Although fresh-frozen human grafts are widely regarded as the gold standard for bone regeneration and demonstrated lower total CFU counts compared to other groups, their ability to promote SCV emergence raises concerns regarding their infection-related risks.

Mimicking implant-associated infections using inoculum composed of metabolically active planktonic bacteria or pre-formed surface-attached biofilms may not accurately represent clinical reality. While high concentrations of planktonic cells can simulate acute infections, pre-grown biofilms fail to reflect the typical scenario immediately following the implantation of a sterile device [67]. In most cases, healthcare-associated infections begin with low-metabolism micro-aggregated bacteria and progress into chronic conditions. To establish a clinically relevant model, *S. aureus* strain S54F9 was cultured for 7 days to produce bacterial micro-aggregates, which were isolated from planktonic cells through filtration and confirmed to be in a low metabolic state by means of IMC (calPlate™, Symcell AB, Stockholm, Sweden). An equal cell density of 1×10^5 CFU/mL was placed in each calorimeter vial, varying only the proportion of planktonic cells and the size of the micro-aggregates. Compared to planktonic cells, micro-aggregated bacteria showed delayed time-to-peak heat flow, likely reflecting the older culture age and lower metabolic activity.

Implant-associated osteomyelitis models were developed in female minipigs using micro-aggregated bacteria (32 μm size) and compared with models inoculated with planktonic cells. An implant cavity was created in the right tibia, into which the inoculum was placed before inserting a sterile stainless-steel implant. Both micro-aggregated bacteria and planktonic cells led to infections affecting the implant, surrounding soft tissue, and bone. However, the micro-aggregated bacteria induced a less-aggressive osteomyelitis, in contrast to the planktonic group, which showed significant osteolysis and purulence. Paradoxically, infections initiated by the micro-aggregated bacteria resulted in good healing with robust osteoid formation, similar to the sham (control) group. These findings highlight the importance of characterizing the metabolic state of bacterial inoculum when designing in vivo models of implant-related infections. Such characterization can also inform in vitro studies of scaffold–microorganism interactions under biorelevant conditions, potentially reducing or replacing the need for animal models [68]. Given the impact of aggregate size and culture age on both heat flow and infection development, the authors recommend reporting inoculum details using the format: Concentration $^{(\text{size; age})}$; for example, $10^{4\ (5\text{–}15\ \mu\text{m};\ 7\ \text{day})}$ CFU.

Microcalorimetry is also suitable to test antiviral drugs [69] and antiparasitic compounds. For instance, IMC allowed measuring antiparasitic drug-induced changes in both metabolic heat production and motor activity of *Schistosoma mansoni* adult worms [70]. By continuously tracking overall heat output, IMC provides a precise assessment of worm viability. Additionally, it quantifies metabolic fluctuations caused by the worm's movements, offering detailed insight into the drug effects.

4. IMC for antimicrobial activity of scaffolds

Microcalorimetry can provide useful information on antibacterial performance of coatings and active substances incorporated to scaffolds and medical devices [71–74]. The minimum inhibitory concentration (MIC) values of several antibiotics estimated through microcalorimetry have been shown to be nearly identical to those measured according to Clinical Laboratory & Standards Institute (CLSI) guidelines. However, IMC offers an additional benefit: at sub-inhibitory concentrations, it clearly distinguishes between bacteriostatic and bactericidal effects [75]. Typically, a bacteriostatic agent decreases μ_m while a bactericidal substance prolongs λ, as observed when testing various drugs against *Mycobacterium* species [76] or copper-loaded cationic particles against *E. coli* and *Candida* spp. [77].

Also, the effects of the essential oil component gallic acid on *S. aureus* growth was effectively assessed using a 3114/3236 TAM Air isothermal microcalorimeter (Thermometric AB, Sweden) by analyzing both the growth rate constant during the second exponential phase and the maximum heat flow output. An inverse relationship was observed for the growth rate constant during the second exponential and gallic acid concentration. Gallic acid began to exhibit inhibitory effects at a concentration of 10 μg/mL, with a 50 % inhibition of bacterial growth at 63.51 μg/mL [52].

Calcium sulfate, commonly used as a bone defect filler, is also widely applied in the treatment of chronic osteomyelitis. Bioabsorbable beads of calcium sulfate with and without gentamicin were challenged against common bone infection pathogens, such as *S. aureus*, *S. epidermidis*, *E. faecalis*, *E. coli* and *C. albicans* in the IMC vials [78]. In the absence of gentamicin, bacterial growth produced the characteristic exponential heat flow curves seen in nutrient-rich conditions (Fig. 4 C1). Conversely, the gentamicin-loaded beads completely suppressed microbial heat production for 24 h, and the IMC plots displayed only the exothermic baseline associated with bead and antibiotic dissolution (Fig. 4 C2). Selecting appropriate controls is key when evaluating antimicrobial activity, as interactions between test materials and growth media can mask or confound results. In posterior studies, IMC was applied to identify the amount of gentamicin that beads made of calcium sulfate and hydroxyapatite should release to completely inhibit planktonic cells, to prevent bacteria adhesion and to completely eradicate biofilms of gram-positive bacteria [79].

Bioactive glasses, commonly used in bone substitute applications, have also been assessed for their antimicrobial activity against key pathogens associated with osteomyelitis using IMC and standard CFU counting [80]. The bioactive glass S53P4 -composed of silica (SiO_2), sodium (Na_2O), calcium (CaO) and phosphate (P_2O_5) ions- was tested in two granulometric forms (<45 μm powder, and 500–800 μm granules)

and at two concentrations (400 and 800 mg/mL). The antimicrobial activity of bioactive glasses is attributed to their capability to release ions and to increase local pH and osmotic pressure. Heat flow was recorded for 24 h in a TAM III (TA Instruments, New Castle, DE, USA) for the S53P4 dispersed in RPMI 1640 medium containing *S. aureus, Staphylococcus epidermidis, Enterococcus faecalis, E. coli* or *Candida albicans* (final concentration of 5 × 10^5 CFUs/mL). Heat flow data (μW) from the first peak in the thermogenesis curve (Fig. 5 A-E) were used to calculate microbial growth rate constants (k, h^{-1}), while total heat production over 24 h (Fig. 5F) reflected overall metabolic activity. The IMC thermogram data revealed a strong effect of the bioactive glasses on the growth rate of microorganisms. The bioactive glass powder (<45 μm) at the highest concentration significantly inhibited bacteria growth, reducing heat production by 60–98 % compared to the positive control recorded in the absence of the bioactive glass. Both granulometric fractions showed strong activity against *C. albicans*, with inhibition rates of 87–97 %. These findings were consistent with the CFU data, which confirmed complete loss of cell viability after 24 h incubation in the presence of the bioactive glass powder.

In a subsequent study, bioactive glass powder and a putty formulation composed of powder particles bound by a synthetic binder demonstrated efficacy against biofilms of methicillin-resistant *S. aureus* (MRSA) and methicillin-resistant *S. epidermidis* (MRSE), without requiring the use of antibiotics (vancomycin) [81]. Collectively, these studies underscore the value of combining IMC and CFU counting for a comprehensive assessment of antimicrobial activity. They also indicate that the efficacy of S53P4 is influenced by particle size, likely due to the greater pH elevation in the surrounding medium caused by smaller particles.

IMC studies specifically focused on biofilm assessment and the impact that scaffold components and antibiotic agents may have on its formation or eradication are still a few [82–84]. The most employed techniques to characterize biofilms are microscopy and culture. However, both present significant limitations. In microscopy, artifacts can arise from incomplete stain penetration within the biofilm matrix, potentially compromising accuracy. Likewise, assessing viability through plate counts is often challenging due to the difficulty of fully detaching the biofilm. IMC has the advantage of providing information on the overall activity of all microorganisms involved in the biofilm without any manipulation or labelling. In microbial cultures without a medical device, biofilm dynamics can be assessed using solid supports like filtration membranes to form colony biofilms. This approach eliminates the use of liquid media, preventing the growth of planktonic cells that could interfere with the evaluation of sessile cell behavior [85].

Sessile bacteria cells embedded in a biofilm formed on a medical device are extremely difficult to eradicate. Therefore, prevention of biofilm formation on healthcare materials is a relevant design criterium when the biomaterials are chosen. For example, surface treatment of titanium implants has been identified as a key factor influencing the risk of biofilm formation in an intraoral human model. Hydrophilic, microroughened surfaces are more susceptible to biofilm development compared to their hydrophobic counterparts, while surface topography

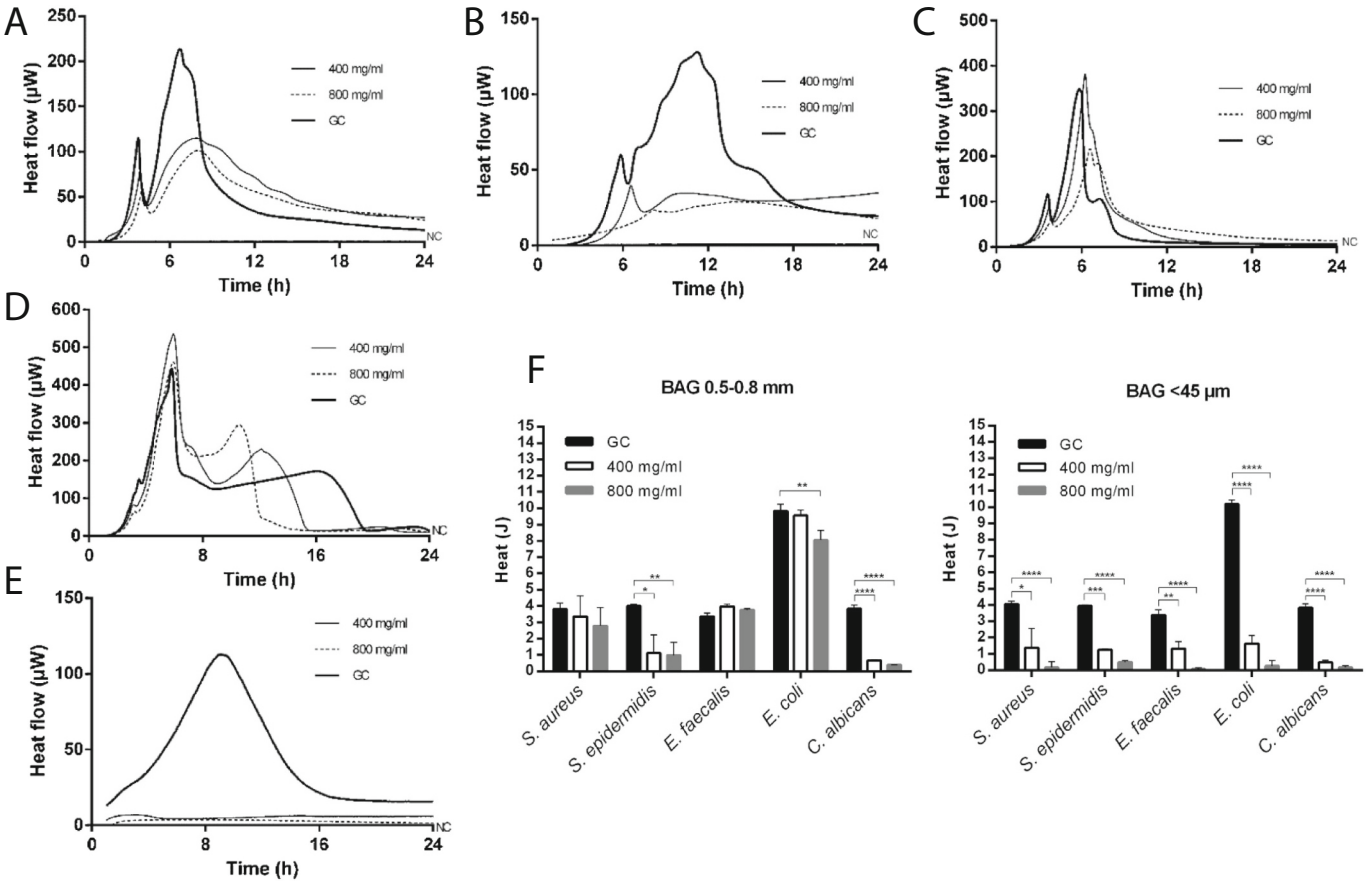

Fig. 5. (A-E) Heat flow curves generated by the metabolic activity of (A) *S. aureus*, (B) *S. epidermidis*, (C) *E. faecalis*, (D) *E. coli* and (E) *C. albicans* in the presence of different concentrations of bioactive glass granules of 500–800 μm. The heat produced by the bioactive glass itself in the same medium was subtracted. Thicker full line represents growth control (GC), thin full line corresponds to 400 mg/mL bioactive glass concentration, dashed line corresponds to 800 mg/mL bioactive glass concentration. Basal line NC represents the negative control (sterile medium). (F) Cumulative heat values were recorded after 24 h incubation in the absence (GC) or presence of bioactive glass granules (500–800 μm) or powder (<45 μm). Statistically significant differences: **** *P* value <0.0001; *** P value 0.0001 to 0.001; ** P value 0.001 to 0.01; * P value 0.01 to 0.05. Adapted from Gonzalez-Moreno et al. [80] with permission of Elsevier.

plays a crucial role in determining cleanability [86].

IMC has also revealed that although staphylococcal biofilm growth is greater on rough surfaces, the subsequent sensitivity to antibiofilm agents, such as daptomycin, is species dependent. For example, minimal biofilm eradication concentration (MBEC) of *S. aureus* on smooth surfaces is lower than on rough surfaces. Differently, the MBEC of *S. epidermidis* did not follow a clear dependence on surface roughness [87]. More recently, it has been shown that coating titanium discs and screws with $Ca(OH)_2$ significantly reduces the risk of biofilm formation, showing lower heat flow and increased lag phase in the IMC assessment [88]. IMC has also been used to demonstrate the usefulness of doping calcium hydroxide and hydroxy apatite coatings with silver to enhance the antimicrobial properties [89].

In a comparative study, bone grafts and bone graft substitutes, such as β-tricalcium phosphate (β-TCP), processed human spongiosa (Tutoplast™), and poly(methyl methacrylate) (PMMA), also including polyethylene (PE), were tested regarding their capability to inhibit biofilm formation when incubated for 24 h with *S. aureus* (9.7×10^5 CFU/mL) and *S. epidermidis* (1.3×10^5 CFU/mL). After incubation and washing, the test materials were sonicated. Sonication fluid was used for bacterial counting, while the sonicated test materials were transferred to sterile 4 mL calorimeter ampoules pre-filled with 1 mL TSB, and the heat flow recorded in 3102 TAM III (TA Instruments, New Castle, DE, USA). Calorimetric time to detection (TTD) was defined as the time from insertion of the ampoule into the calorimeter until the exponentially rising heat flow signal exceeded 75 μW for *S. epidermidis* and 100 μW for *S. aureus* (Fig. 6A). TTD indirectly quantifies the number of bacteria, with a shorter TTD representing a larger amount [90].

The peak heat flow (PHF) was defined as the maximum heat flow during the experiment, and the time to reach the peak heat flow (ttPHF) was recorded. PHF is correlated with two factors: (i) linearly with the volume of growth medium added to the ampoules; and (ii) in case of equal volumes of growth medium individual to the strain [90]. β-TCP showed the highest bacterial load per sample (*S. aureus*: 7.67 ± 0.17; *S. epidermidis*: 8.14 ± 0.05 $\log_{10}$ cfu), whereas PMMA exhibited the highest bacterial density per surface area (*S. aureus*: 6.12 ± 0.2; *S. epidermidis*: 7.65 ± 0.13 $\log_{10}$ cfu). Biofilm formation by *S. aureus* was detected significantly faster on porous materials (β-TCP and processed human spongiosa) than on smooth surfaces (PMMA and PE). In contrast, for *S. epidermidis*, detection times differed significantly across nearly all materials, except between processed human spongiosa and PE, which exhibited an intermediate behavior. IMC data (Fig. 6A) agreed well with the CFU counting and proved to be an effective, non-invasive method for real-time monitoring of bacterial biomass, enabling detection without physically disturbing the biofilm.

Regarding synthetic calcium phosphates (CaP) bone grafts, it has been shown that β-tricalcium phosphate (β-TCP), α-TCP, dicalcium phosphate (DCP) and calcium-deficient hydroxyapatite (CDHA) are all susceptible to colonization by *S. aureus* and *S. epidermidis* [91]. Biofilm formation was assessed by incubating CaP grafts for 3, 24, or 72 h in

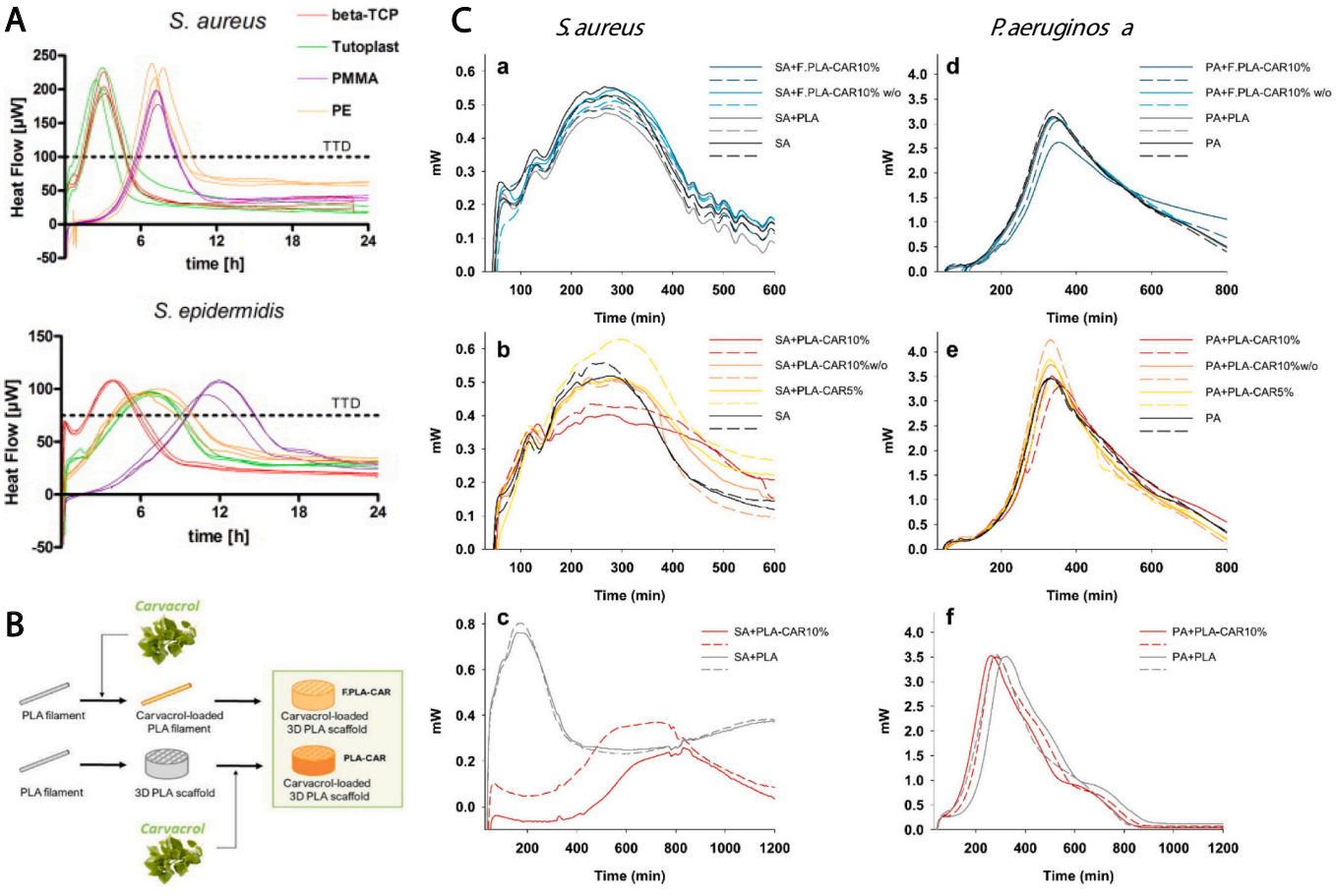

Fig. 6. (A) IMC thermograms for *S. aureus* and *S. epidermidis* cultured on bone grafts and bone graft substitutes ($n = 3$). Dotted line indicates time to detection (TTD) for *S. aureus* (100 μW) and *S. epidermidis* (75 μW). Reproduced from Clauss et al. [90] with permission of Elsevier. (B) Scheme of the preparation of carvacrol-loaded 3D printed PLA bone implants by incorporating carvacrol to PLA filament before 3D printing (F.PLA-CAR scaffold), or by swelling the 3D printed scaffold in carvacrol solution (PLA-CAR scaffold); and (C) IMC thermograms for scaffolds incubated (a,b,c) with *S. aureus* (OD 0.1) and (d,e,f) with *P. aeruginosa* (OD 0.01). Some scaffolds (a,b,d,e) were incubated with the bacteria inoculum directly (since $t = 0$ min) in the calorimeter vials. Another scaffolds (c,f) were first incubated with the bacteria for 6 h in a well-plate and then washed with fresh medium and transferred to calorimeter vials containing culture medium ($n = 2$ per condition). Reproduced from Farto-Vaamonde et al. [94] with permission of Elsevier.

bacterial suspension (1.0–1.5 × 10^5 CFU/mL) prepared in either tryptic soy broth (TSB) or undiluted pooled human serum. Following incubation, the grafts were washed (to remove planktonic bacteria), sonicated (half of the grafts), and analyzed (all grafts) in a TAM III microcalorimeter. All CaP grafts showed less biofilm formation, measured in terms of lower CFU/mL and longer TTD, when incubated in serum compared to TSB. Biofilm formation demonstrated a complex dependence on various physicochemical properties, including pore size, specific surface area, and total porosity of the grafts. Therefore, isolating the effect of any single property remains challenging, as controlling for all other variables simultaneously is still unresolved. In a subsequent in vivo study, infected bone grafts were implanted subcutaneously and explanted after 3, 24, and 72 h. Under these conditions, not only the structural properties of the material but also changes in surface composition and topology resulting from protein adsorption were shown to influence the heat flow thermograms [92].

IMC has been used to monitor the effects of incorporating amphotericin B into PMMA bone cements for the treatment of fungal prosthetic joint infections (PJI). Notably, differences in drug release rates due to the use of liposomal versus non-liposomal formulations, as well as the inclusion of various porogens, significantly influenced the performance and therapeutic potential of the PMMA bone cements [93].

To avoid the misuse of antibiotics, various essential oil components have been incorporated to implantable scaffolds with the aim of preventing infections while avoiding the risk of generating resistances. Carvacrol is a natural low-cost compound derived from oregano which presents anti-bacterial and anti-biofilm properties against both gram-positive and gram-negative bacteria. Carvacrol-loaded PLA scaffolds were prepared via 3D printing to promote bone tissue regeneration while preventing biofilm formation [94]. Scaffolds were printed with or without a perimeter wall to mimic the cortical structure of bone and evaluate whether the lateral interconnectivity influenced biological or antimicrobial properties. Carvacrol was incorporated using two strategies: (i) pre-printing by loading the PLA filament (scaffolds coded as F. PLA-CAR), or (ii) post-printing by soaking the printed scaffolds in carvacrol solutions (coded as PLA-CAR) (Fig. 6B). The incorporation method affected carvacrol distribution and release profiles. While both showed biphasic release, post-printed scaffolds released 50–80 % of carvacrol within the first 24 h, whereas pre-loaded filaments sustained the release over several weeks. The presence of a perimeter did not alter the release rate but influenced the total amount released. Tissue integration and vascularization were assessed in a chorioallantoic membrane model (CAM) model using a quantitative micro-computed tomography (micro-CT) approach.

Antibiofilm activity against *S. aureus* and *Pseudomonas aeruginosa* was evaluated by CFU counting after biofilm detachment and in-real time using an I-Cal Flex isothermal calorimeter system (Calmetrix, Needham, MA, USA) equipped with 8 calorimeters at 37 °C. Scaffolds were incubated with culture medium either alone (control) or inoculated with bacteria (*S. aureus* at OD 0.1; *P. aeruginosa* at OD 0.01). Control experiments using sterile scaffolds in bacteria-free media confirmed (i) that carvacrol release did not itself produce significant heat signals, and (ii) that the scaffolds were sterile over 48 h (signals remained in the −0.02 to +0.02 mW range). The IMC plots recorded for the bacteria cultures revealed a rapid initial growth rate both in the absence and the presence of the scaffolds (Fig. 6C a.b,d,e), with a notably high heat output for *P. aeruginosa*. Only PLA-CAR 10 % scaffolds with perimeter notably impacted on bacterial metabolism: for *S. aureus*, heat flow was significantly reduced, and for *P. aeruginosa*, a delayed metabolic peak was observed. These changes suggest the carvacrol released from the scaffold altered bacterial activity. Blank PLA scaffolds had no effect, and PLA-CAR 10 % without perimeter were less effective—likely due to lower carvacrol content. F.PLA-CAR scaffolds (loaded before printing) showed no perimeter-related differences, possibly due to their slower carvacrol release [94].

In other sets of experiments, PLA and PLA-CAR 10 % scaffolds were incubated with bacterial suspensions for 6 h, then washed to remove planktonic cells, leaving only adhered biofilms. These biofilm-laden scaffolds were placed into calorimeter vials containing fresh medium (TSB-1 for *S. aureus*, LB for *P. aeruginosa*) and monitored for 48 h at 37 °C (Fig. 6C c,f). In line with turbidity measurements, when the scaffolds were washed to remove non-adhered *S. aureus* cells, PLA-CAR 10 % scaffolds showed reduced and delayed heat flow, consistent with low bacterial counts and contact-killing effects. In contrast, blank PLA scaffolds generated strong signals, indicative of active bacterial growth. No significant calorimetric changes were observed for *P. aeruginosa*, suggesting limited efficacy of carvacrol against this species under the tested conditions [94].

In this line, thymol and zinc ions were combined to enhance the antibiofilm properties of polysaccharide-based porous wound dressings fabricated via semi-extrusion 3D printing [95]. Thymol, a monoterpenoid naturally found in *Thymus vulgaris*, is classified as Generally Recognized as Safe (GRAS) by the FDA and has demonstrated antibacterial and antibiofilm activity, particularly against Gram-positive bacteria, in addition to its anti-inflammatory and pro-healing effects. Zinc salts are also known for their broad-spectrum antimicrobial activity against both gram-positive and gram-negative bacteria [96]. Mixtures of xanthan gum (XG) and guar gum (GG) were optimized as printable inks. To solubilize hydrophobic thymol in the aqueous formulation, hydroxypropyl-β-cyclodextrin (HPβCD) was incorporated as a host molecule. The resulting thymol-loaded dressings were subsequently loaded with Zn^{2+} via ionic complexation with XG, which also contributed to reinforcing the structural integrity of the printed scaffolds. The antimicrobial efficacy of thymol-loaded dressings, with and without Zn^{2+}, was evaluated against *S. aureus*, *P. aeruginosa*, and *S. epidermidis* using IMC and quantification of viable biofilm-associated cells. For the IMC assays, 3 mL of bacterial inoculum (*S. aureus* and *S. epidermidis* O.D. 0.1, *P. aeruginosa* O.D. 0.01) was added to calorimeter tubes, and one dressing was placed in each tube. Tubes containing only the inoculum served as control. Power output (mW) was recorded for 72 h for *S. aureus* and *S. epidermidis* and 24 h for *P. aeruginosa* (I-Cal Flex isothermal calorimeter, Calmetrix, Needham, MA, USA). Two calorimeter cells per experiment monitored bacterial growth in the absence of scaffolds, while others assessed metabolic heat production in the presence of dressings. All tests were performed in duplicate. After calorimetry, scaffolds were removed, rinsed with PBS, and then sonicated for 15 min and vortexed for 30 s. The resulting supernatants were used to determine the number of CFUs as a measure of biofilm formation (Fig. 7) [95].

Complex formation of thymol with HPβCD was found to be critical for achieving effective thymol concentrations. However, both IMC thermograms and CFU counts indicated that thymol-only dressings (S-T7+ and S-T14+) showed limited activity against *S. aureus* and *S. epidermidis*, which grew quite well on pristine dressings (S-NT) (Fig. 7 A1, D1). In contrast, dressings containing Zn^{2+} solely (S-Zn) or combined with thymol (S-TZn) significantly reduced the metabolic activity of *S. aureus* and *S. epidermidis* compared to controls (Fig. 7 B1, D1), while the effect on *P. aeruginosa* was less pronounced (Fig. 7 C1). In the latter case, a modest antibacterial effect was noted during the declining phase of the metabolic heat curve, with a ~ 2.5-h advancement relative to controls. The addition of thymol to the Zn^{2+}-loaded dressing (S-TZn) did not significantly enhance antibacterial activity against *P. aeruginosa* compared to S-Zn alone (Fig. 7 C1, C2), as confirmed by reductions of 3.76 Log (99.98 %) and 3.91 Log (99.99 %) for S-Zn and S-TZn, respectively. However, a synergistic antibiofilm effect was observed against gram-positive bacteria when thymol and Zn^{2+} were combined (Fig. 7 D1, D2). For *S. aureus*, S-Zn achieved a ~ 2.9 Log reduction (99.87 %) in biofilm formation, whereas S-TZn led to a ~ 3.3 Log reduction (99.95 %). Similarly, in *S. epidermidis*, S-Zn reduced biofilm by 1.16 Log (93.08 %), and S-TZn by 1.76 Log (98.26 %). These findings evidence that gram-positive bacteria, particularly *S. aureus*, are more susceptible to thymol's antimicrobial and antibiofilm effects, while the antibiofilm action against *P. aeruginosa* is primarily attributed to the

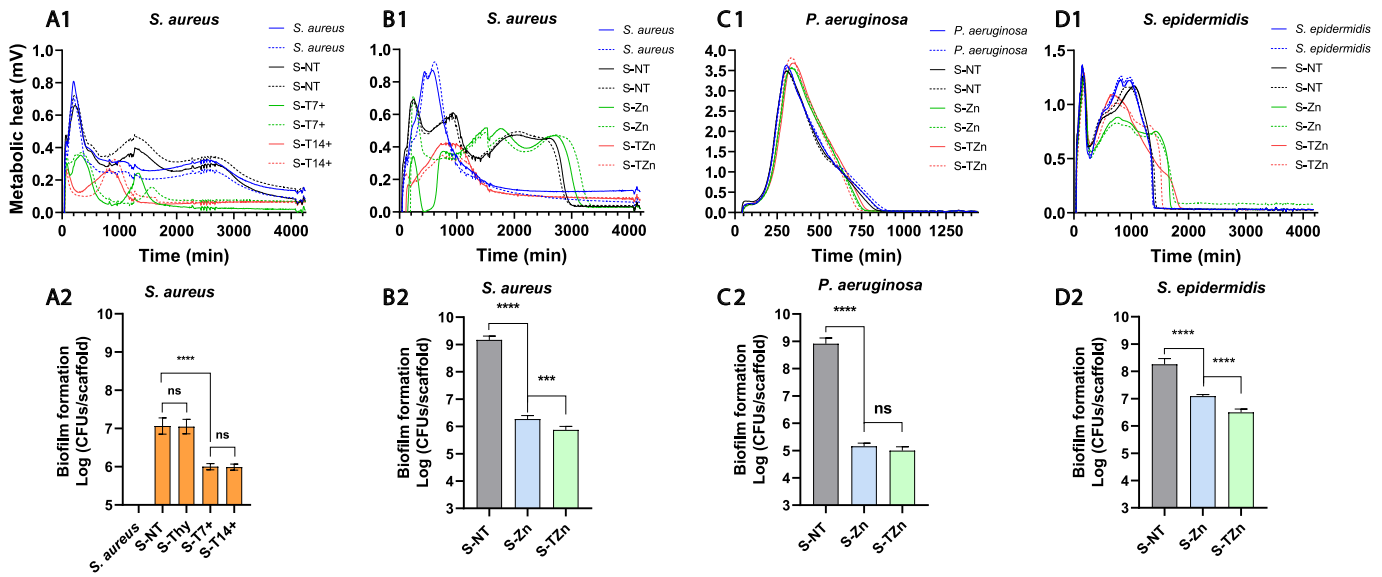

Fig. 7. Isothermal microcalorimetry runs carried out at 37 °C for (A1) *S. aureus* (initial O.D. 0.1) cultured in tryptic soy broth (TSB) with non-loaded scaffold (S-NT) and thymol-loaded (low dose S-T7+ and high dose S-T14+) scaffolds, (B1) *S. aureus* (initial O.D. 0.1) cultured in TSB with non-loaded scaffold (S-NT), zinc-loaded (S-Zn) and dually thymol and zinc-loaded (S-TZn) scaffolds, (C1) *P. aeruginosa* (initial O.D. 0.01) cultured in Luria-Bertani's lysogenic broth with or without S-NT, S-Zn, and S-TZn scaffolds, and (D1) *S. epidermidis* (initial O.D. 0.1) cultured in TSB with or without S-NT, S-Zn, and S-TZn scaffolds. Two replicates are shown for all microcalorimeter graphs for each condition (solid and dotted lines). (A2, B2, C2 and D2) CFU quantification of biofilm formation after incubation in the microcalorimeter. One way ANOVA (with Brown Forsythe, and Shapiro-Willis): $p < 0.05$; 0.1234 (ns), 0.0332 (*), 0.0021 (**), 0.0002 (***), <0.0001 (****), $n = 6$. Reproduced from Virzì et al. [95] with permission of Elsevier. (For interpretation of the references to colour in this figure legend, the reader is referred to the web version of this article.)

presence of Zn^{2+}.

Biofilm-associated bacteria exhibit significantly reduced susceptibility to antibiotics compared to their planktonic counterparts. This prompted the incorporation of bacteriophages into a variety of medical devices, mainly dressings for chronic wounds and staphylococcal implant-associated infections [97]. ICM has been shown to be a convenient technique to evaluate the specificity of novel bacteriophages against a variety of clinically relevant bacteria [98–100].

S. aureus-specific bacteriophage Sb-1 was evaluated solely and in conjunction with various antibiotics regarding its capability to inhibit the biofilm of methicillin-resistant *S. aureus* (MRSA) and to target persister cells [101]. The study used an isothermal 48-channel batch calorimeter (TAM III, TA Instruments, USA) to assess the antimicrobial activity of antibiotics against both planktonic and biofilm bacterial forms. For the planktonic assay, bacterial cells were inoculated in nutrient media with antibiotics at varying concentrations, and heat production (indicative of metabolic activity/growth) was monitored over 24 h. For the biofilm assay, bacteria were first grown on porous glass beads to form biofilms, then treated with antibiotics. After treatment, beads were transferred to fresh media to monitor any remaining bacterial activity via heat production over 48 h. Growth controls and negative controls (sterile beads) were included. Specific supplements (calcium chloride or glucose 6-phosphate) were added depending on the antibiotic used.

The authors defined Minimum Heat Inhibitory Concentration (MHIC) as the lowest antimicrobial concentration inhibiting heat production in planktonic bacteria after 24 h; Minimum Biofilm Bactericidal Concentration (MBBC) as the lowest antimicrobial concentration preventing heat production from biofilms after 48 h, indicating no bacterial regrowth; and Minimum Biofilm Eradicating Concentration (MBEC) defined as the lowest antimicrobial concentration required to eradicate the biofilm [101,102]. To assess the impact of combined treatment with an antibiotic and Sb-1 on biofilm-embedded cells, mature biofilms were first established on beads. After washing, the beads were incubated in BHI broth containing sub-eradicating concentrations or titers of the antibiotic and Sb-1 for 24 h at 37 °C. Additionally, the effects of sequential exposure—24 h with Sb-1 followed by 24 h with the antibiotic, and vice versa—were investigated. In all scenarios, the heat flow generated by viable biofilm-associated cells was monitored over 48 h using calorimetric analysis (Fig. 8).

Microcalorimetric analysis showed that while Sb-1 phage at 10^7 PFU/mL significantly reduced MRSA biofilm viability, it did not fully eradicate the biofilm, consistent with previous in vivo studies on implant-related infections [103]. A single phage dose often fails to eliminate in vitro biofilms due to the protective biofilm matrix and dormant cells. Combining phages with antibiotics—especially rifampin or daptomycin—resulted in synergistic biofilm eradication, marking the first report of such synergy between Sb-1 and daptomycin (Fig. 8). Sequential treatment, particularly phage pre-exposure followed by antibiotics, was more effective than simultaneous administration. Synergistic effects were observed for rifampin, daptomycin, fosfomycin, vancomycin, and ciprofloxacin when preceded by Sb-1. Thus, Sb-1 pretreatment enabled clinically achievable antibiotic doses to eradicate biofilm, even when co-treatment failed. Sb-1 appeared to degrade the biofilm matrix, aiding antibiotic penetration. A "Trojan horse" effect was observed: phage-infected persister cells lysed upon returning to active growth, reducing relapse risk. Subsequent IMC studies carried out with biofilms of ten rifampin-resistant *S. aureus* clinical strains [104] confirmed that Sb-1 enhances the efficacy of various antibiotics against MRSA biofilms, particularly with staggered application (first Sb-1 for 24 h followed by antibiotic), which support further in vivo research to optimize phage–antibiotic combination therapies for persistent infections.

Notably, IMC has also demonstrated the effectiveness of a sequential antibiotic treatment in fully eradicating MRSA biofilms [105]. In this approach, vancomycin was first used to eliminate metabolically active cells, followed by daptomycin to target the remaining persister cells. After vancomycin treatment, approximately 5 % of the bacterial population survived in a metabolically inactive state (persisters). These cells remained dormant until exposed to fresh, antibiotic-free medium, at which point they reverted to a metabolically active state within 24 h. This study highlights the importance of re-evaluating biofilms to detect

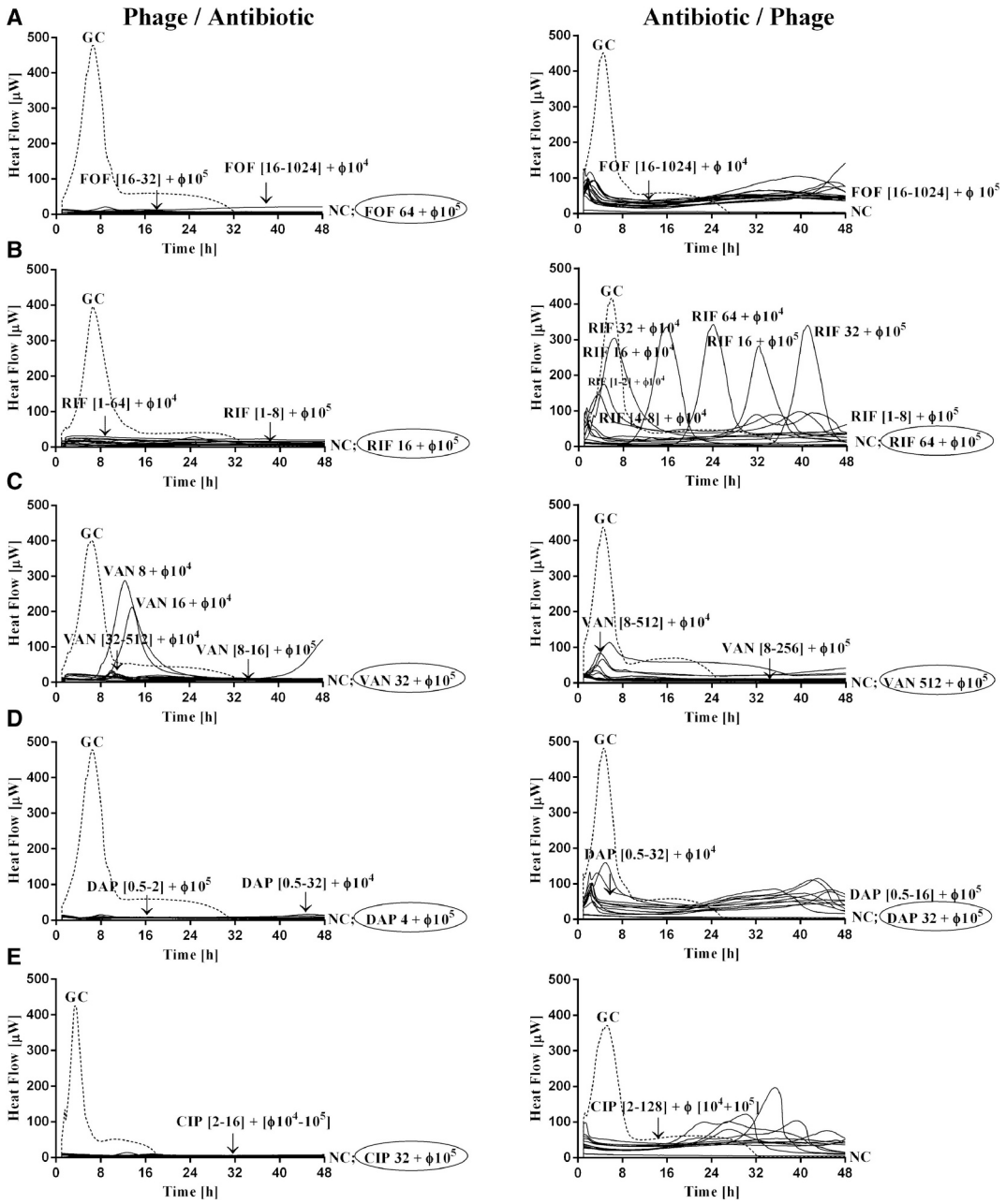

Fig. 8. Microcalorimetric evaluation of methicillin-resistant *S. aureus* (MRSA) ATCC 43300 biofilms was performed following staggered treatment with Sb-1 and antibiotics. The graphs on the left depict the effect of Sb-1 followed by antibiotic exposure, while those on the right show the reverse sequence. Antibiotics tested included fosfomycin (FOF) (A), rifampin (RIF) (B), vancomycin (VAN) (C), daptomycin (DAP) (D), and ciprofloxacin (CIP) (E). Each curve represents heat production by viable biofilm-associated bacteria post-treatment. Untreated controls (GC) were included for comparison. Combinations were tested using fixed antibiotic concentrations at fractions of the Minimum Biofilm Eradicating Concentration (MBEC) (1/4 to 1/256) and subinhibitory titers of Sb-1 (10^4 or 10^5 PFU/mL). Values above each curve indicate antibiotic concentrations (µg/mL) and Sb-1 titers (PFU/mL). Circled values mark the MBEC, defined as the lowest antibiotic concentration resulting in no bacterial regrowth after 48 h and no colonies following sonication and plating. GC (dashed line) represents the growth control; NC denotes the negative control. Reproduced from Tkhilaishvili et al. [101] with permission of Elsevier.

surviving cells that may contribute to persistent healthcare-associated infections in vivo. It also demonstrates the effectiveness of IMC as a valuable tool for identifying treatments targeting persister cells.

Recently, phage therapy has shown promise in treating fracture-related infections through a dual delivery system composed of hydrogel and alginate microbeads. This system delivers both a phage cocktail and the antibiotic meropenem, targeting multi-drug resistant *Pseudomonas aeruginosa* [100]. To evaluate antimicrobial activity, biofilms were grown on glass beads and treated with either phages, antibiotics at varying concentrations (1×, 10×, and 100× MIC), or a combination of both. Sequential treatments—phage followed by antibiotic—were also tested. Antibacterial efficacy was assessed using IMC to measure heat production by viable bacteria and CFU counts after biofilm disruption by sonication. Results showed that higher phage titers enhanced the antibiotic's effectiveness, while lower titers were less impactful. IMC and CFU analyses provided complementary insights into bacterial viability and biofilm recovery. Two phages, FJK.R9–30 and MK.R3–15, demonstrated synergistic activity with meropenem against biofilms. The combined antimicrobial effect remained stable for up to eight days at body temperature within the hydrogel-microbead system (PA-HM). In a

mouse model of fracture-related infection, phages delivered via PA-HM were recovered from all tissues. Moreover, animals treated with PA-HM showed reduced phage resistance and lower levels of immune system neutralization compared to those receiving phages in saline.

An alternative to bacteriophage therapy is the development of novel antimicrobial peptides (AMPs) that can be used in combination with antibiotics to produce synergistic effects. Several AMPs —SAAP-148, acyldepsipeptide-4, LL-37, and pexiganan— were evaluated regarding their anti-biofilm and anti-persister efficacy against PJI. MRSA biofilm models simulating PJI were developed on acetabular hip liners and metal alloys (titanium, niobium, and aluminum) that are used in prosthetic joints [106]. Mature biofilms were exposed daily to rifampicin and ciprofloxacin for three days, achieving a 4-log reduction in bacterial load. To prevent the reactivation of persister cells, AMP treatment began immediately after antibiotic exposure. Potential regrowth was assessed by inspecting bacterial colonies on agar plates after five days of incubation. In this study, IMC was only used for real-time monitoring of heat flow by MRSA in antibiotics-treated mature biofilms formed on TAN (titanium-aluminum-niobium) disks using a CalScreener® calorimeter (Symcel Sverige, Sweden). Heat flow readings were nearly undetectable in pretreated biofilms, indicating that the persister cells are metabolically inactive. Among the tested AMPs, SAAP-148 and pexiganan were identified in this study as the most effective, rapidly eliminating biofilm-residing bacteria in a dose-dependent manner.

Interestingly, IMC has also been employed to validate sonication of explanted medical devices as an effective strategy for biofilm removal from implant surfaces for diagnostic purposes. Compared to chemical agents used for biofilm dislodgment, sonication enabled the recovery of a greater number of colonies from biofilms of *S. epidermidis* (ATCC 35984), *S. aureus* (ATCC 43300), *E. coli* (ATCC 25922), and *P. aeruginosa* (ATCC 53278) grown on porous glass beads [107].

In sum, IMC yields MIC values consistent with CLSI standards while uniquely distinguishing bacteriostatic from bactericidal effects at sub-inhibitory concentrations. It enables non-invasive, real-time monitoring of bacterial biomass and biofilms, with strong agreement to CFU counts. IMC also supports evaluation of bacteriophage specificity and treatments targeting persister cells, while informing in vitro and in vivo infection models under biorelevant conditions. These features highlight IMC as a versatile tool for antimicrobial development and infection biology.

5. IMC for monitoring biomaterials and scaffolds formation and physicochemical stability

One of the major advantages of microcalorimetry is its ability to analyze virtually any type of specimen, ranging from liquids to solids. Biomaterials and scaffold samples can be directly placed into a microcalorimeter ampoule without extensive preparation. By continuously measuring heat flow relative to appropriate controls, microcalorimetry enables the quantification of both the rate and extent of physical and chemical degradation processes, such as hydrolysis and corrosion. Unlike differential scanning calorimetry (DSC), which typically subjects samples to elevated temperatures over short periods (often far above those encountered during normal use or storage), IMC allows for the monitoring of slow reactions over extended periods under tightly controlled environmental conditions. These can include variables such as medium composition, pH, oxygen levels, and relative humidity [108]. Although IMC typically requires larger sample sizes—on the order of one gram, compared to the milligram quantities used in DSC—it offers superior sensitivity. This enables precise monitoring of the stability of both solutions and solid materials under real-world storage conditions, rather than under the accelerated conditions typically used in DSC. As a result, IMC allows for the direct determination of reaction rate constants at the temperature of interest, eliminating the need to conduct tests at elevated temperatures (which may alter the degradation mechanism) and avoiding reliance on extrapolation via the Arrhenius Eq. [109].

IMC also offers advantages over high-performance liquid chromatography (HPLC), a technique commonly used to monitor the chemical stability of active substances and polymers. Unlike HPLC, which requires the dissolution of the test material, IMC enables direct analysis of solids and intact formulations. In solution-based testing, HPLC often struggles to simultaneously detect subtle decreases in the concentration of the parent compound and the corresponding increases in degradation products, which is why accelerated stability conditions are frequently employed. Additionally, dissolving a stored solid for HPLC analysis erases physical changes in the material internal structure, potentially obscuring important stability information. Several studies have highlighted the advantages of IMC for monitoring drug stability and drug-material interactions [110].

A clear example of the suitability of IMCs to determine the physicochemical stability of implantable materials is that of ultra-high molecular weight polyethylene (UHMWPE). This polymer serves as a key bearing surface in hip, knee, and other joint replacement implants. The sterilization method used before implantation significantly impacts the material's long-term stability, as slow oxidative degradation occurs over months or years, affecting its mechanical properties. Gamma (γ) irradiation, a common sterilization method, generates free radicals in UHMWPE, accelerating oxidation unless counteracted (e.g., by adding α-tocopherol). This oxidation leads to embrittlement, reducing wear and fracture resistance, ultimately compromising the implant's clinical performance. Several microcalorimetric studies have investigated UHMWPE stability. One study found that the physicochemical stability of γ-radiation sterilized UHMWPE was five to nine times lower than that of ethylene oxide (EtO)-sterilized material [111]. Researchers attributed this decreased stability to a combination of oxidation due to free radical reactions and hydrolytic degradation in oxidized polymer regions.

To further investigate the stability of UHMWPE exposed to air, heat flow rates were measured at 20, 25, 35, and 45 °C for non-sterilized, γ-radiation sterilized and EtO-sterilized samples. IMC curves were used to estimate the activation energies, which were 47, 11, and 41 kJ/mol, respectively. The heat flow plots confirmed exothermic reactions in γ-radiation sterilized UHMWPE, suggesting that in vivo, the surface of articular components made from this material may become oxidized during wearing [112].

The impact of sterilization on the stability of acrylic bone cements has also been demonstrated using IMC [113]. The exothermic heat flow (Q) of Palacos® R acrylic bone cement powder exposed to ambient air was monitored over a period of up to 200 h. Four powder variants were assessed: unsterilized, EtO-sterilized, and γ-irradiated at doses of 2.5 and 4.5 Mrad. Each was evaluated after being stored under ambient conditions for 2 days, 3 weeks, and 9 months post-sterilization. Best-fit models of Q as a function of time were used to calculate an "effective" heat flow (Q_{eff}) over the interval of 14–200 h. The Q_{eff} values of unsterilized and EtO-sterilized powders were consistently low and remained stable across all storage durations. In contrast, γ-irradiated powders exhibited significantly higher Q_{eff} when tested 2 days post-sterilization, indicating reduced thermal stability; however, these differences were no longer evident after 3 weeks or 9 months of storage. These results suggest that EtO-sterilized bone cement powders are thermally stable and can be safely used in cemented arthroplasties immediately after sterilization, regardless of shelf storage time. In comparison, γ-irradiated powders require a minimum of three weeks of ambient storage to achieve similar stability before clinical use [114].

IMC is particularly suitable for monitoring bone cement formation, particularly calcium phosphate-based cements, where setting and curing times are critical. If the cement sets too quickly, its strength and toughness can be compromised. Like many solid-state reactions, cement hydration cannot be accurately described using standard chemical rate equations (e.g., first-order or second-order kinetics). However, distinct phases of the setting process can be identified: an initial rapid reaction (often undetectable in IMC due to the time needed for thermal equilibration), followed by a lag phase, then a sharp increase in reaction rate,

and finally, a gradual decline in activity [115,116]. IMC allows researchers to monitor the setting process over extended periods and to assess how additives impact the setting reactions of bone cements to improve strength and other properties. DSC, when operated in isothermal mode, has also been used for such studies. The relatively longer time needed in the IMC to first achieve thermal equilibration, compared to DSC, compromises the capture of the initial stages of the process, but it can be solved with the use of injection systems and mixers that enable the addition of the liquid component once the calorimeter is stabilized.

In conclusion, IMC provides a powerful, non-destructive means to quantify both the rate and extent of physical and chemical degradation processes of biomaterials and scaffolds under physiologically relevant conditions. Beyond monitoring degradation, IMC can also assess the energetic changes introduced during scaffold preparation and sterilization, including the storage and subsequent release of energy, which may influence host tissue responses following implantation.

6. IMC for evaluation of mammalian cells and tissues

IMC has been shown to be particularly useful to monitor the activity (including replication) of low number of mammalian cells in culture (10^4–10^5) and to investigate the interactions between cells and biomaterials. Numerous mammalian cells and cell cultures have been analyzed for their heat production and metabolic activity using IMC [28,117]. For instance, thermogenesis in adipocytes has been investigated in both rat and human cells [118–120]. In vitro studies on adipocytes derived from obese patients have suggested that changes in cellular metabolic efficiency play a crucial role in obesity pathogenesis [121]. Similarly, research on hepatocytes has demonstrated that microcalorimetry is a useful tool for studying carbohydrate and fat metabolism in cultured cells. However, discrepancies in heat production rates between cells cultured in vitro and those in vivo were found [122].

IMC has also been applied to living tissue samples, such as dissected or biopsy-derived tissues, for research and diagnostic purposes. For example, propranolol and other β-blocker drugs have been shown to have an impact on muscle thermogenesis and endurance. It has been reported that muscle biopsies from a patient who had taken propranolol for one week showed reduced thermogenesis and lower isokinetic endurance [123]. Subsequent research in both human and animal models confirmed these findings, highlighting differences between propranolol and other drugs such as terbutaline [124] and carvedilol [125]. Beyond muscle studies, IMC has also been used to analyze urogenital tract biopsies, effectively distinguishing tumorous from non-tumorous tissues [126]. By comparing histological findings with calorimetric data, researchers demonstrated that heat production measurements could be used to grade tumor malignancy, as further developed in section 7.

An important caution when analyzing biopsies with IMC is the risk of microbial growth. For example, in a study with 152 colon biopsies from healthy individuals incubated in various nutrient media, bacterial growth altered enthalpy values in the absence of antibiotics. The addition of gentamicin was necessary to prevent such artifacts and to measure heat flow originating solely from human tissue [30]. Additionally, IMC has revealed marked differences in collagenase-mediated degradation of biological tissues when fresh compared with those fixed by glutaraldehyde or ethylene glycol diglycidyl ether; fresh tissues released significantly more heat, consistent with their greater degree of degradation [127].

In tissue engineering, microcalorimetry has emerged as a valuable technique for monitoring the growth and proliferation of human cell lines under varying culture conditions. For instance, studies involving CHO320 hamster ovarian cells have shown that this method can facilitate the optimization of cell culture media [128]. CHO320 cells genetically engineered to produce interferon-γ exhibited changes in heat flow corresponding to nutrient availability and the accumulation of toxic metabolic byproducts. These findings underscore the utility of IMC in the rational design of culture conditions for biopharmaceutical production [129].

Research has shown that the growth of primary human chondrocytes can be effectively tracked in a microcalorimetric ampoule, and that early IMC-measured growth rates correlate well with long-term cell expansion under standard conditions—traditionally assessed through time-consuming cell counts [130]. This suggests that IMC offers a simple and efficient alternative for evaluating the expansion potential of donor-derived cells. It can also be applied to track the activity of microencapsulated cells [131]. Since IMC is non-destructive, high-value samples can be recovered intact for further biochemical, histological, and mechanical analyses. For example, when studying chondrocytes, samples removed from the calorimeter can be analyzed post-IMC for cell viability and DNA content using standard kits [130], as well as for the biochemistry, tissue structure, and mechanical properties of newly formed cartilage.

Moreover, IMC applications extend beyond culture optimization and may serve as an alternative to animal models in preclinical biocompatibility and safety testing [132,133]. For instance, IMC demonstrated the effects of Cr(VI) on human dermal fibroblasts, which are implicated in severe skin ulcerations. Control cells exhibited a heat production of 15 ± 5 pW per cell, whereas exposure to 0–500 μM Cr(VI) progressively inhibited heat production over 3–25 h. The IC_{50} was determined to be 29 ± 4 μM, in close agreement with the conventional colorimetric WST-1 assay (35 ± 5 μM) [134]. These results demonstrate that Cr(VI) impairs fibroblast metabolism and induces cell death, highlighting the utility of microcalorimetry for toxicity assessment. In a subsequent study with other metal ions, combining IMC and oximetry, Cd(II) exposure inhibited both thermogenesis and cell respiration, whereas Ni(II) had no detectable effect and Al(III) selectively inhibited respiration without altering thermogenesis. After 24 h at 40 μM, Cd(II) caused fibroblasts death, whereas Al(III) and Ni(II) appeared to overstimulate the cells, increasing thermogenesis and respiration [135]. These findings can inform the design of metal-containing hip implants by considering the tissue ion levels reached under normal and excessive wear conditions.

IMC was used to study gentamicin's effects on human blood cell metabolism. At concentrations above therapeutic levels, the drug increased heat production in red cells and slightly in granulocytes, while lymphocytes were unaffected. No effects were observed at lower concentrations, confirming microcalorimetry as a useful tool for assessing drug impact on cellular metabolism [136].

Potential cytotoxic effects of the 63S bioactive glass (produced using the sol-gel method) and hydroxyapatite (HA, extracted from bovine bone) were assessed using yeast (*Saccharomyces cerevisiae*) and human chondrocyte cells in a micro calorimeter TAM48 (Waters/TA) (Fig. 9) [137]. XRD analysis revealed that the bioactive glass had an amorphous structure, whereas HA was fully crystalline. *Saccharomyces cerevisiae* maintained normal growth in YPD medium with bioactive glass concentrations up to 3.3 mg/mL (10 mg/vial). At higher concentrations, yeast showed reduced metabolic activity and delayed growth, with complete inhibition at 50 mg (Fig. 9 A1). HA did not negatively affect yeast growth up to 6.6 mg/mL (20 mg/vial), and only mild delays were observed at higher levels, with significant inhibition appearing at 15.5 mg/mL (Fig. 9 A2). Human chondrocyte cells showed no major adverse effects when exposed to 3 mg of either bioactive glass or HA, with only a slight drop in metabolic activity (Fig. 9 A3). Growth patterns remained consistent across cultures, with decline attributed to the closed nature of the IMC vial, which lacks nutrient renewal. No heat flow was detected in the negative control, verifying that all recorded activity was due to cell-biomaterial interactions. The study showed that yeast cells, being easier to manipulate, could serve as an effective preliminary model for estimating conditions suitable for human cell assays [137].

IMC has also been explored for its ability to monitor the heat produced during macrophage phagocytosis of particulate materials. These particles may result from surface wear of metal or polymer prostheses or

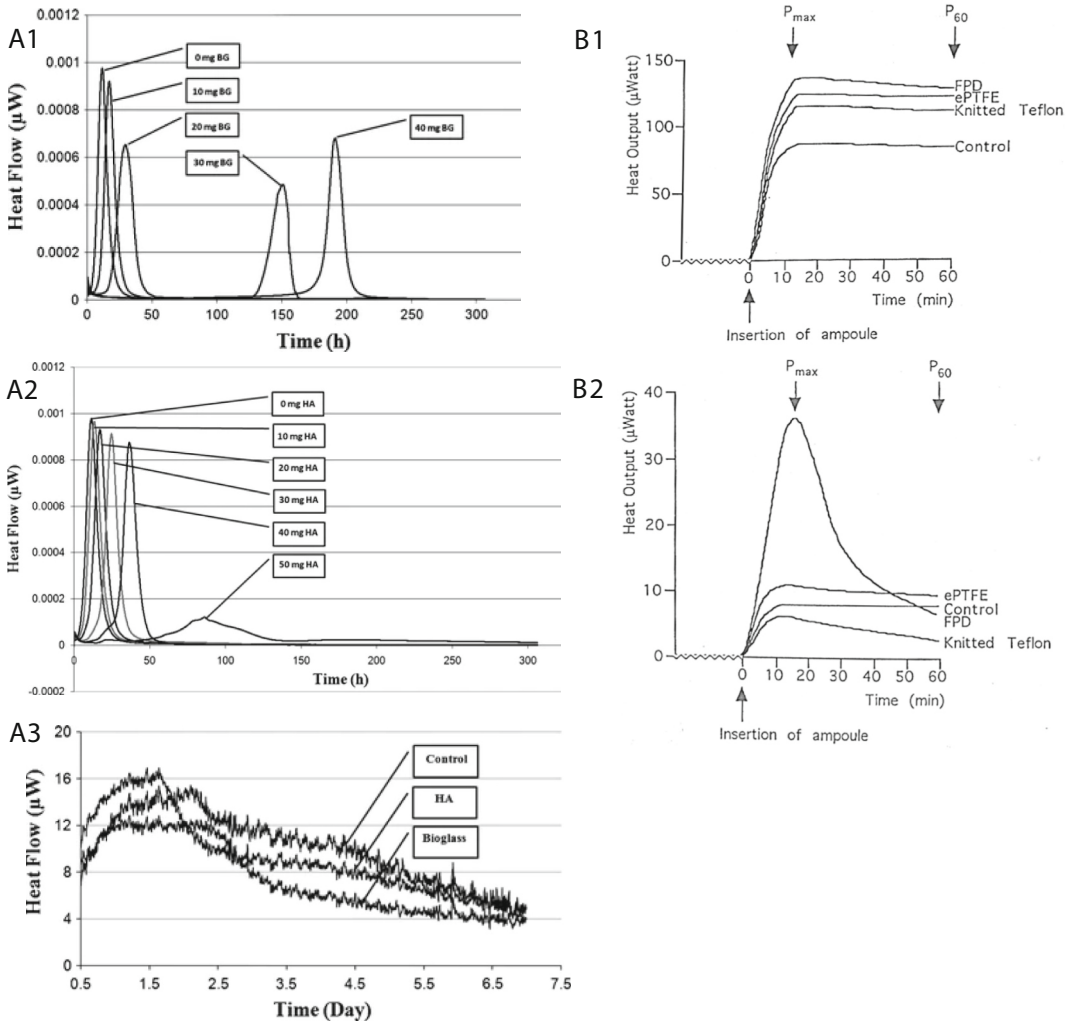

Fig. 9. (A) Heat flow curves showing the effect of (A1) bioactive glass particles (BG) on *Saccharomyces cerevisiae* growth (O.D. <0.05) in yeast peptone dextrose (YPD) medium, (A2) hydroxyapatite (HA) particles on *S. cerevisiae* growth (O.D. <0.05) in yeast peptone dextrose (YPD) medium, and (A3) bioactive glass and HA particles (3 mg) on cultured human chondrocyte cells growth in Dubelco's modified eagle's medium. BG composition was 63 mol% SiO_2, 28 mol% CaO, 9 mol% P_2O_5. Reprinted from Doostmohammadi et al. [137] with permission of Springer Nature. (B) Heat flow curves of (B1) platelet-concentrate suspensions (1175 ± 125 × 10^6/mL) and (B2) leukocyte suspensions (1 × 10^6/mL) incubated with Fluorometer Passivated Dacron (FPD), expanded polytetrafluoroethylene (ePTFE) and knitted Teflon vascular grafts and without (control). Reprinted from Swartbol et al. [141] with permission of Sage Publications.

scaffolds. Their presence can trigger an inflammatory response, potentially shortening the lifespan of the device and, in the case of bone implants, leading to osteolysis. Preliminary studies have shown that substrates with lipopolysaccharide (LPS) bound to the surface induce an increase in heat flow from macrophages. Tests using both inorganic and organic microparticles also demonstrated elevated heat flow compared to particle-free controls, although the specific impact of surface-bound LPS remains unclear [138]. IMC also evidenced an increase in heat flow when splenic lymphocytes were exposed to ginseng and astralagus, probably because the activation of immune mechanisms, such T cell receptor and PI3 K-Akt signaling pathways [139].

Non-nucleated cells, such as red blood cells (RBC), have also been evaluated in the calorimeter. It was shown that RBCs account for 50 % of the total head output of blood, whereas lymphocytes, granulocytes, and platelets account for 20 %, 20 %, and 10 %, respectively [140]. Variations in the rate of heat production by blood cells may serve as an indicator of various diseases. For example, an increased heat production rate in erythrocytes has been associated with anemia.

IMC has been employed to assess the metabolic response of human platelets and leukocytes when exposed to synthetic vascular graft materials [141]. Cell accumulation on the inner surface of small-diameter vascular grafts can lead to complications such as thrombosis, intimal hyperplasia, and eventual occlusion. The study compared three types of grafts: expanded polytetrafluoroethylene (ePTFE), knitted Teflon and Fluorometer Passivated Dacron (FPD) grafts. FPD was made by adding a fluoro-polymer layer onto a knitted Dacron to reduce thrombogenicity and leukocyte activation. When exposed to any of the graft materials, platelets exhibited a rapid increase in metabolic activity, which then stabilized and remained steady for over one hour (Fig. 9 B1). Leukocyte responses, however, varied with the material: neither ePTFE nor knitted Teflon induced significant metabolic activity, while FPD triggered a pronounced heat flow peak within the first 15 min of contact (Fig. 9 B2). This suggests that FPD causes strong leukocyte activation, though the underlying mechanisms were not further investigated in the study.

In a follow-up study, the metabolic responses of granulocytes and platelets to modified knitted Dacron vascular grafts were examined and compared to those elicited by untreated grafts [142]. The grafts were either collagen-impregnated or externally coated with collagen. Collagen impregnation significantly increased cell adhesion and resulted in the highest heat production; that is, up to four times greater than that of the other graft types within 30 min. This observation aligns with in vivo findings showing that small-diameter grafts internally coated with

collagen are highly thrombogenic.

The activity of organelles such as mitochondria, when isolated from cells, can be effectively monitored using IMC [143]. Thermogenic and thermokinetic profiles of mitochondria can provide valuable insights into inter- and intra-species genetic differences, as well as the effects of pharmacological agents or other treatments [144]. While there are currently no published studies specifically investigating mitochondrial heat flow perturbations caused by scaffolds, research involving gadolinium-based contrast agents has shown that Gd^{3+} salts exert a concentration-dependent effect on mitochondrial energy metabolism. This finding helps to explain the observed toxicity associated with high concentrations of these contrast agents [145].

In sum, IMC is a powerful, non-invasive tool for assessing the metabolic activity of mammalian cells and tissues. It allows real-time monitoring of viability, proliferation, and biomaterial interactions while preserving samples for further analysis. By enabling such measurements in vitro, IMC supports the 3R's principles by reducing and refining the use of animal models in tissue engineering and biomedical research.

7. IMC for evaluation of antitumoral treatments

Several studies highlighted a correlation between tumor cell malignancy and cellular heat production rates, with malignant cells generating more metabolic heat than normal cells. First evidence referred to lymphocytes from individuals with non-Hodgkin's lymphoma, which exhibited elevated heat production [146]. At the tissue level, research on biopsies from urogenital tract organs has demonstrated that IMC can rapidly differentiate between tumorous and non-tumorous samples [147]. The diagnostic findings obtained through IMC in this study aligned well with results from histological analysis and impulse cytophotometry.

Many molecular alterations in tumor cells contribute to what is known as metabolic reprogramming, but the most significant changes typically involve glycolysis and the tricarboxylic acid (TCA) cycle in conjunction with the oxidative phosphorylation (OXPHOS) system. These pathways are the primary sources of ATP in tumor cells [148]. Based on their predominant energy-producing pathways, tumor cells are generally categorized as either glycolytic (relying heavily on aerobic glycolysis) or oxidative, where OXPHOS is recruited to meet increased energy demands. However, classifying tumors strictly as glycolytic or oxidative is challenging due to their metabolic complexity. A more straightforward approach involves examining the bioenergetics of tumor and metastatic cells through a fundamental and universal parameter: thermogenesis. Using isothermal microcalorimetry, researchers identified thermogenic differences among various cell lines and correlated these with specific metabolic pathways and the organelles responsible for adaptive thermogenesis [149,150]. Cell lines were selected based on their metastatic potential, which ranked as follows. Tongue carcinoma: LN-2 > LN-1 > SCC-9; Murine melanoma: 4C11+ > 4C11− > 4C; Human melanoma: WM852 > WM9838B > WM983A; Breast cancer: MDA-MB-231 > MCF-7; and Lung cancer: H460 > A549.

Heat production was measured using an OMEGA Isothermal Titration Calorimeter (VP-ITC, Microcal Inc., Northampton, MA). After equilibration at 37 °C, the experiment was initiated by injecting intact cells—or, in some cases, cell-free extracts—into the sample chamber. Heat changes were recorded every 5 min over a 35-min period. Each measurement involved injecting 120 μL of a cell suspension containing 1.2×10^5 cells. Although each tumor type displayed a distinct heat release profile, the most thermogenic cells were consistently those with the highest metastatic potential (e.g., 4C11+, WM852, H460, LN-2, and MDA-MB-231). Moreover, mitochondrial extracts from metastatic cells exhibited significantly higher thermogenic activity compared to those from non-metastatic cells [149]. Overall, the use of isothermal titration microcalorimetry provided a non-invasive, real-time, and highly sensitive method to quantify the net energy output of living tumor cells, offering valuable insights into their metabolic behavior and metastatic potential.

Flow microcalorimetry was applied to measure dihydrofolate reductase (DHFR) activity in rat and human malignant tissue homogenates. Unlike conventional assays, its sensitivity enables direct detection in crude preparations. In rats, liver showed the highest DHFR activity, while lung and brain had lower levels, with optimal pH values of 4.5 for liver and 6.8 for lung and brain. Enzyme activity increased 1.5–3-fold with 0.6 M KCl or NaCl. Low DHFR activity was also detected in human bone tumor homogenates, highlighting the method's potential for enzyme analysis in malignant tissues [151].

Microcalorimeters adapted for use with 48-well microtiter plates have also proven suitable for monitoring the growth of hepatocarcinoma microtissues (approximately 1000 cells per microtissue), demonstrating a linear relationship between thermal power output and the number of microtissues per well [150]. A similar microcalorimeter has been used for the fast screening of the efficacy of new drug candidates against rare childhood tumors [152] and neuroblastoma [153].

Changes in intestinal microbiota have been shown to occur during cancer progression. Specific microbial community has been associated with greater morbidity and poor prognosis of cancer, but it has also been shown that certain tumors alter the diversity of the microbial communities [154–156]. An engineered resistant-starch (ERS) diet, in which corn starch was replaced with resistant starch, was evaluated as an alternative to fasting to investigate the effects of dietary restriction on pancreatic cancer development. Due to the indigestibility of resistant starch, the ERS diet resulted in reduced intestinal glucose concentrations. Its impact on fecal microbiota was assessed using IMC in nude mice before and after pancreatic cancer induction. Compared to a control diet, the ERS diet led to increased microbial diversity and a higher relative abundance of *Lactobacillus* species in the pre-cancer fecal microbiota. Following cancer induction, microbial diversity declined in both groups. Before cancer induction, acetate was the predominant fermentation product, whereas after induction, propionate production became more pronounced. Mice on the ERS diet showed lower total acid production overall. These microbiota shifts were reflected in the IMC scans, which generally showed reduced total heat accumulation [157]. These findings suggest that IMC could serve as a useful tool to correlate dietary interventions with cancer progression.

Other studies have also demonstrated that the addition of glucose or fructose to cancer cell cultures notably increases the heat flow, indicating elevated metabolic activity. As mentioned above, high metabolic activity is associated with an increased metastatic potential compared to non-migrating cells. As an example, neuroblastoma cells exhibited an enhanced thermogenic profile in the presence of fructose, which appears to support cell survival under conditions of low oxygen and limited nutrient availability [158]. IMC may enable the classification of tumor cells into high or low metastatic potential groups based on their thermogenic profiles.

IMC studies on tumor cell apoptosis have demonstrated that increasing the temperature from 37 to 42.5 °C leads to a reduction in the metabolic activity of tumor cells. These findings provide valuable insight into the mechanisms underlying the effectiveness of scaffolds with photothermotherapy capabilities for localized tumor eradication. Furthermore, this knowledge may contribute to the development of optimized clinical protocols—specifically regarding temperature threshold and application duration—to enhance the efficacy of thermotherapy, whether used alone or in combination with chemo- and radio-therapy. Human ovarian carcinoma cell line (COCL) (3.28×10^5 cells in 1 mL) were incubated at 37, 40, 42.5 and 43.5 °C in a LKB 2277 Bioactivity Monitor microcalorimeter. No changes in heat flow were observed at 40 °C with respect to 37 °C, but a strong decrease was recorded at 42.5 °C and more markedly at 43.5 °C in a 24-h time frame period. Addition of a chemotherapeutic drug notably shortened the time for the heat flow decline and made the decrease more pronounced, showing that the simultaneous application of hyperthermia and

chemotherapy caused synergic effect on cell apoptosis [159].

In sum, IMC offers a sensitive, non-invasive means to assess tumor bioenergetics, linking thermogenesis with malignancy, metastatic potential, and treatment response. Unlike conventional assays, it enables real-time monitoring of intact samples with minimal preparation. These advantages make IMC a valuable translational tool for drug screening, microbiota and dietary studies, and the optimization of hyperthermia-based therapies.

8. Conclusions and a view to the future

Measuring the energy associated with biological events has long been recognized as a key approach to understanding their underlying mechanisms. Advances in technology over the past two centuries now allow the detection of extremely small heat flows, such as those generated by the metabolism of just a few cells. Among calorimetric techniques, IMC stands out for its ability to monitor thermal events under constant temperature and tightly controlled environmental conditions that can closely mimic the in vivo environment of damaged tissues or implantation sites.

While interpreting calorimetric data typically requires validation through complementary methods, IMC patterns offer immediate qualitative insights when comparing biomaterials or cell–material interactions under standardized conditions. Quantitative information can also be extracted using simple mathematical models. Readers interested in these models are referred to previous reports [33,38,49,54,160].

A major strength of IMC is its versatility: it can analyze virtually any sample type, from liquids to solids. Biomaterials or scaffold samples can be directly placed into microcalorimeter ampoules, enabling continuous recording of heat flow relative to controls. Physical degradation processes (e.g., hydrolysis, corrosion) and biological interactions, including bacterial or mammalian cell adhesion, can be quantified in terms of both rate and extent. IMC has proven valuable for rapid sterility screening of scaffolds and implantation sites, emphasizing the importance of characterizing the metabolic state of bacterial inocula when designing in vivo models of implant-related infections. These insights can guide in vitro studies under biorelevant conditions, potentially reducing or replacing animal testing.

IMC can also aid in rapid diagnostic of infections in implantable devices. Importantly, such early detection—achievable within just a few hours compared to traditional microbiological methods—could have substantial clinical impact. Establishing antimicrobial therapy before biofilm development is critical, as once biofilms form, bacteria become highly resistant to antibiotic treatment. Early calorimetric detection may therefore play a pivotal role in reducing patient complications associated with healthcare-related infections.

IMC also enables assessment of antibacterial performance of coatings and active compounds incorporated into scaffolds and medical devices, supporting classification of materials based on biofilm risk or eradication capability. IMC is particularly effective for evaluating natural antimicrobial agents and bacteriophages as alternatives or adjuncts to antibiotics against multidrug-resistant bacteria. Unlike conventional end-point assessments conducted after a few hours of culture, IMC allows real-time monitoring of metabolic changes and relapses over time, identifying persister cells. The technique also reveals structural changes in scaffolds caused by sterilization methods, such as prolonged energy release after gamma irradiation.

Although studies on mammalian cell growth on scaffolds during tissue regeneration remain limited, IMC can detect metabolic changes in response to pharmacological or physical stimuli. Applications extend beyond optimizing cell culture conditions, offering potential as a non-animal model for preclinical biocompatibility and safety testing. For instance, IMC can monitor macrophage responses to particles shed from scaffolds, immune reactions to biomaterials, or hemolysis. IMC can also quantify the net energy output of tumor cells, providing insight into their metabolic state, metastatic potential, and how interventions—including scaffold-based therapies—alter tumor progression.

Although still in early development, innovations such as microfluidic calorimetric chips offer promising opportunities for integrating IMC with microfluidics under flow conditions that more closely mimic in vivo environments [161,162]. The advantages and disadvantages of currently developed closed and open microcalorimeter chips have recently been reviewed [163]. Future IMC systems may further benefit from miniaturization and improved stabilization, enabling the study of scaffold–cell interactions (both mammalian and microbial) under fluctuating temperatures that mimic physiological rhythms (e.g., sleep, exercise) or pathological conditions such as fever. As a proof-of-concept a microfluidic chip capable of measuring bacterial growth through heat flux in a thermally non-stabilized environment (with temperature fluctuations of ~1 K) has been shown effective for monitoring early bacteria proliferation before biofilm formation. This finding opens promising avenues for the rapid detection of infections in implantable devices. Importantly, such early detection—achievable within just a few hours compared to traditional microbiological methods—could have substantial clinical impact. Establishing antimicrobial therapy before biofilm development is critical, as once biofilms form, bacteria become highly resistant to antibiotic treatment. Early calorimetric detection may therefore play a pivotal role in reducing patient mortality associated with healthcare-related infections [162].

Multi-well IMC also represents a significant advance, providing incipient high-throughput screening capabilities [150]. Reports on multi-well IMC are rapidly increasing, demonstrating its reliability for characterizing a variety of mammalian cells [164,165] and microorganisms and parasitic worms [150,166] across diverse biomedical applications. For instance, thin-film sensors integrated into the bottom of standard 96-well plates have enabled real-time, label-free monitoring of both cell number and metabolic activity [167]. More recently, although not strictly IMC, a multi-parameter sensing platform was developed to combine thermal and impedance measurements in a microplate format. Thermal signals reflect biomass, while impedance captures viability-related membrane integrity. Using *S. cerevisiae*, multivariate models predicted cell number and viability with errors of 0.106×10^{7} cells and 19.67 %, improving to 5.02 % at higher cell concentrations [168]. This integrated approach outperformed single-parameter methods and enables real-time monitoring for applications in bioprocessing, drug screening, and toxicity testing.

In parallel, the development of ultrasensitive microcalorimeters offers tools for bioanalysis at the droplet, single-cell, or even subcellular level [163].

In addition to technical innovations, the choice of vessel material is crucial for reliable IMC measurements. Vessels must avoid altering cell metabolism while ensuring rapid heat transfer for stable and accurate measurements. Previous studies showed that human granulocytes and phagocytes are artificially activated by contact with stainless steel vessels, producing elevated and variable heat signals. Lining the vessels with fluoroethylene-polypropylene eliminates this effect, enhancing the accuracy of microcalorimetry for assessing granulocyte metabolism under physiological in vitro conditions [169]. Consequently, titanium, glass or plastic vials are now commonly preferred.

Recent studies have demonstrated IMC's ability to measure energy expenditure in small invertebrates (e.g., *Caenorhabditis elegans*) [170] and vertebrates (e.g., zebrafish larvae) [171], supporting evaluation of scaffold regenerative potential while aligning with the 3Rs principle by reducing reliance on animal models. This capability is particularly relevant in the context of FDA Modernization Acts 2.0 and 3.0, which formally recognize validated nonclinical methods as alternatives to animal testing. FDA Modernization Act 2.0 [172] permits the use of validated non-animal alternatives in preclinical testing of drugs and biological products, while FDA Modernization Act 3.0 [173] emphasized the development of human biology–based models. IMC can support both approaches, especially when biorelevant, disease-specific models are

integrated into assay vials. Heat flow signatures of biomaterials or medical devices may even serve as indicators of quality and performance.

The development of IMC applications in the biomedical field could be significantly advanced if authors consistently included the keywords "microcalorimetry" or "isothermal microcalorimetry" in their publications. At present, many papers employing the technique either omit it from the title and keywords or use a diverse range of terms to describe the same technology. Adopting a more uniform approach to keyword usage—specifically including IMC—would greatly enhance the discoverability of relevant research and support the continued growth of the field.

By enabling real-time, non-destructive, and multiparametric monitoring of cell viability, microbial proliferation, and scaffold performance under physiologically relevant conditions, IMC exemplifies the vision of Industry 5.0, which emphasizes human-centric, sustainable, and intelligent innovation. Its ability to generate high-quality, reproducible data supports ethical, human-relevant preclinical testing while reducing reliance on animal models. Incorporating IMC into standardized workflows can advance personalized, efficient, and sustainable scaffold design and drug evaluation, bridging cutting-edge technology with patient-centered outcomes. Broader adoption and validation of IMC could accelerate translational research while embodying the human- and sustainability-focused goals of Industry 5.0.

Declaration of AI-assisted technologies in the writing process

AI-assisted technologies (chat-GPT) were used in the writing process before submission, but only to improve the language and readability of the manuscript. After using this tool, the authors reviewed and edited the content as needed and took full responsibility for the content of the published article.

CRediT authorship contribution statement

Carmen Alvarez-Lorenzo: Writing – review & editing, Writing – original draft, Visualization, Validation, Software, Resources, Methodology, Formal analysis, Data curation, Conceptualization. **Angel Concheiro:** Writing – review & editing, Writing – original draft, Resources, Methodology, Formal analysis, Data curation, Conceptualization.

Funding

The work was supported by Spain Ministerio de Ciencia, Innovación y Universidades MICIU/AEI/ 10.13039/501100011033 [PID2023-150422OB-I00], ERDF A way of making Europe, cofunded by the European Union, and Xunta de Galicia [ED431C 2024/09].

Declaration of competing interest

The authors declare that they have no known competing financial interests or personal relationships that could have appeared to influence the work reported in this paper.

Data availability

No original data were used.

References

[1] Farag MM. Recent trends on biomaterials for tissue regeneration applications: review. J Mater Sci 2023;58:527–58. https://doi.org/10.1007/s10853-022-08102-x.
[2] van Daal M, de Kanter AFJ, Bredenoord AL, de Graeff N. Personalized 3D printed scaffolds: the ethical aspects. N Biotechnol 2023;78:116–22. https://doi.org/10.1016/j.nbt.2023.10.006.
[3] Breque M, De Nul L, Petridis A. Industry 5.0: Towards a sustainable, humancentric and resilient European Industry. European Commission; 2021. https://msu.euramet.org/current_calls/documents/EC_Industry5.0.pdf.
[4] Iyengar KP, Zaw Pe E, Jalli J, Shashidhara MK, Jain VK, Vaish A, et al. Industry 5.0 technology capabilities in trauma and orthopaedics. J Orthop 2022;32:125–32. https://doi.org/10.1016/j.jor.2022.06.001.
[5] Haleem A, Javaid M. Industry 5.0 and its expected applications in medical field. Curr Med Res Pract 2019;9:167–9. https://doi.org/10.1016/j.cmrp.2019.07.002.
[6] Jeyaraman M, Nallakumarasamy A, Jeyaraman N. Industry 5.0 in Orthopaedics. JOIO 2022;56:1694–702. https://doi.org/10.1007/s43465-022-00712-6.
[7] Suamte L, Tirkey A, Barman J, Jayasekhar Babu P. Various manufacturing methods and ideal properties of scaffolds for tissue engineering applications. Smart Materials in Manufacturing 2023;1:100011. https://doi.org/10.1016/j.smmf.2022.100011.
[8] Alvarez-Lorenzo C, Goyanes A, Concheiro A. Cyclodextrins in 3D/4D printing for biomedical applications. Addit Manuf 2024;84:104120. https://doi.org/10.1016/j.addma.2024.104120.
[9] Las Heras K, Garcia-Orue I, Rancan F, Igartua M, Santos-Vizcaino E, Hernandez RM. Modulating the immune system towards a functional chronic wound healing: a biomaterials and nanomedicine perspective. Adv Drug Deliv Rev 2024;210:115342. https://doi.org/10.1016/j.addr.2024.115342.
[10] Gamba A, Napierska D, Zotinca A. Measuring and reducing plastics in the healthcare sector. Brussels: HCWH Europe; 2021. https://europe.noharm.org/sites/default/files/documents-files/6886/2021-09-23-measuring-and-reducing-plastics-in-the-healthcare-sector.pdf.
[11] Moshkbid E, Cree DE, Bradford L, Zhang W. Biodegradable alternatives to plastic in medical equipment: current state, challenges, and the future. J Compos Sci 2024;8:342. https://doi.org/10.3390/jcs8090342.
[12] Chinga-Carrasco G, Ehman NV, Filgueira D, Johansson J, Vallejos ME, Felissia FE, et al. Bagasse—a major agro-industrial residue as potential resource for nanocellulose inks for 3D printing of wound dressing devices. Addit Manuf 2019;28:267–74. https://doi.org/10.1016/j.addma.2019.05.014.
[13] Zhou T, Wu J, Hu X, Cao Z, Yang B, Li Y, et al. Microplastics released from disposable medical devices and their toxic responses in *Caenorhabditis elegans*. Environ Res 2023;239(Part 1):117345. https://doi.org/10.1016/j.envres.2023.117345.
[14] Serrano-Aroca A, Cano-Vicent A, Sabater I, Serra R, El-Tanani M, Aljabali A, et al. Scaffolds in the microbial resistant era: fabrication, materials, properties and tissue engineering applications. Mater Today Bio 2022;16:100412. https://doi.org/10.1016/j.mtbio.2022.100412.
[15] Trinh KTL, Lee NY. Recent methods for the viability assessment of bacterial pathogens: advances, challenges, and future perspectives. Pathogens 2022;11:1057. https://doi.org/10.3390/pathogens11091057.
[16] Horakova J, Klicova M, Erben J, Klapstova A, Novotny V, Behalek L, et al. Impact of various sterilization and disinfection techniques on electrospun poly-ε-caprolactone. ACS Omega 2020;5:8885–92. https://doi.org/10.1021/acsomega.0c00503.
[17] Tao M, Ao T, Mao X, Yan X, Javed R, Hou W, et al. Sterilization and disinfection methods for decellularized matrix materials: review, consideration and proposal. Bioact Mater 2021;6:2927–45. https://doi.org/10.1016/j.bioactmat.2021.02.010.
[18] Gaisford S. Isothermal microcalorimetry. In: Müllertz A, Perrie Y, Rades T, editors. Analytical techniques in the pharmaceutical sciences. Advances in delivery science and technology. New York, NY: Springer; 2016. https://doi.org/10.1007/978-1-4939-4029-5_12.
[19] Braissant O, Wirz D, Göpfert B, Daniels AU. Biomedical use of isothermal microcalorimeters. Sensors 2010;10:9369–83. https://doi.org/10.3390/s101009369.
[20] Kenny GP, Notley SR, Gagnon D. Direct calorimetry: a brief historical review of its use in the study of human metabolism and thermoregulation. Eur J Appl Physiol 2017;117:1765–85. https://doi.org/10.1007/s00421-017-3670-5.
[21] Da Poian AT, El-Bacha T, Luz MRMP. Nutrient utilization in humans: metabolism pathways. Nature Education 2010;3:11. https://www.nature.com/scitable/content/ice-calorimeter-developed-by-lavoisier-and-laplace-14898943/.
[22] Archiza B, Welch JF, Sheel AW. Classical experiments in whole-body metabolism: closed-circuit respirometry. Eur J Appl Physiol 2017;117:1929–37. https://doi.org/10.1007/s00421-017-3681-2.
[23] Skolik RA, Konkle ME, Menze MA. Calorespirometry: a powerful, noninvasive approach to investigate cellular energy metabolism. J Vis Exp 2018;135:e57724. https://doi.org/10.3791/57724.
[24] Calmetrix. https://www.calmetrix.com/i-cal-flex;; 2025. accessed April 2025.
[25] Wadsö I, Hallén D, Jansson M, Suurkuusk J, Wenzler T, Braissant O. A well-plate format isothermal multi-channel microcalorimeter for monitoring the activity of living cells and tissues. Thermochim Acta 2017;652:141–9. https://doi.org/10.1016/j.tca.2017.03.010.
[26] Guan YH, Lloyd PC, Kemp RB. A calorimetric flow vessel optimised for measuring the metabolic activity of animal cells. Thermochim Acta 1999;332:211–20. https://doi.org/10.1016/S0040-6031(99)00076-3.
[27] Braissant O, Daniels AU. Closed ampoule isothermal microcalorimetry for continuous real-time detection and evaluation of cultured mammalian cell activity and responses. In: Stoddart MJ, editor. Mammalian cell viability: Methods and protocols, methods in molecular biology. vol. 740. Springer Science +Business Media, LLC; 2011. p. 191–208. https://doi.org/10.1007/978-1-61779-108-6_20.

[28] Kemp RB, Guan YH. Heat flux and the calorimetric-respirometric ratio as measures of catabolic flux in mammalian cells. Thermochim Acta 1997;300:199–211. https://doi.org/10.1016/S0040-6031(96)03125-5.
[29] Loesberg C, van Miltenburg JC, van Wuk R. Heat production of mammalian cells at different cell-cycle phases. J Thermal Biol 1982;7:209–13. https://doi.org/10.1016/0306-4565(82)90026-2.
[30] Pocha Ch, Kehrer G, Eitner K, Otto A, Singer D, Bosseckert H. Methodic problems in microcalorimetric measurements of human colonic mucosa. Thermochim Acta 1997;291:15–20. https://doi.org/10.1016/S0040-6031(96)03111-5.
[31] Popa MG, Muntean AA, Popa VT, Dragomirescu CC, Eremia I, Nica S, et al. Microcalorimetric growth evaluation of *Candida albicans* in different conditions. Rom Biotechnol Lett 2020;25:2140–7. https://doi.org/10.25083/rbl/25.6/2140.2147.
[32] Fricke C, Harms H, Maskow T. How to speed up the detection of aerobic microbial contaminations by using isothermal microcalorimetry. J Therm Anal Calorim 2020;142:1933–49. https://doi.org/10.1007/s10973-020-09986-0.
[33] Nykyri J, Herrmann AM, Håkansson S. Isothermal microcalorimetry for thermal viable count of microorganisms in pure cultures and stabilized formulations. BMC Microbiol 2019;19(2019):65. https://doi.org/10.1186/s12866-019-1432-8.
[34] Johansson P, Wadso I. An isothermal microcalorimetric titration/perfusion vessel equipped with electrodes and spectrophotometer. Thermochim Acta 1999;342:19–29. https://doi.org/10.1016/S0040-6031(99)00299-3.
[35] Bonnet M, Lagier JC, Raoult D, Khelaifia S. Bacterial culture through selective and non-selective conditions: the evolution of culture media in clinical microbiology. New Microbes New Infect 2019;34:100622. https://doi.org/10.1016/j.nmni.2019.100622.
[36] Khalef N, Campanella O, Bakri A. Isothermal calorimetry: methods and applications in food and pharmaceutical fields. Curr Opin Food Sci 2016;9:70–6. https://doi.org/10.1016/j.cofs.2016.09.004.
[37] Popa M, Cursaru A, Popa V, Munteanu A, Şerban B, Creţu B, et al. Understanding orthopedic infections through a different perspective: microcalorimetry growth curves. Exp Ther Med 2022;23:263. https://doi.org/10.3892/etm.2022.11189.
[38] Braissant O, Bachmann A, Bonkat G. Microcalorimetric assays for measuring cell growth and metabolic activity: methodology and applications. Methods 2015;76:27–34. https://doi.org/10.1016/j.ymeth.2014.10.009.
[39] Falconer RJ, Schuur B, Mittermaier AK. Applications of isothermal titration calorimetry in pure and applied research from 2016 to 2020. J Mol Recognit 2021;34:e2901. https://doi.org/10.1002/jmr.2901.
[40] Farkas P, Lőrinczy D. New possibilities of application of differential scanning calorimetry-new clinical diagnostic methods on the horizon? Temperature (Austin) 2017;4:120–2. https://doi.org/10.1080/23328940.2017.1292164.
[41] Gill P, Moghadam TT, Ranjbar B. Differential scanning calorimetry techniques: applications in biology and nanoscience. J Biomol Tech 2010;21:167–93.
[42] Guan YH, Lloyd PC, Kemp RB. A calorimetric flow vessel optimised for measuring the metabolic activity of animal cells. Thermochim Acta 1999;332:211–20. https://doi.org/10.1016/S0040-6031(99)00076-3.
[43] Khalef N, Campanella O, Bakri A. Isothermal calorimetry: methods and applications in food and pharmaceutical fields. Curr Opin Food Sci 2016;9:70–6. https://doi.org/10.1016/j.cofs.2016.09.004.
[44] Wadsö I. Isothermal microcalorimetry in applied biology. Thermochim Acta 2002;394:305–11. https://doi.org/10.1016/S0040-6031(02)00263-0.
[45] Braissant O, Wirz D, Goepfert B, Daniels AU. Use of isothermal microcalorimetry to monitor microbial activities. FEMS Microbiol Lett 2010;303:1–8. https://doi.org/10.1111/j.1574-6968.2009.01819.x.
[46] Fricke C, Harms H, Maskow T. Rapid calorimetric detection of bacterial contamination: influence of the cultivation technique. Front Microbiol 2019;10:2530. https://doi.org/10.3389/fmicb.2019.02530.
[47] Corvec S, Seiler E, Wang L, Gonzalez Moreno M, Trampuz A. Characterization of medical relevant anaerobic microorganisms by isothermal microcalorimetry. Anaerobe 2020;66:102282. https://doi.org/10.1016/j.anaerobe.2020.102282.
[48] Brueckner D, Krähenbühl S, Zuber U, Bonkat G, Braissant O. An alternative sterility assessment for parenteral drug products using isothermal microcalorimetry. J Appl Microbiol 2017;123:773–9. https://doi.org/10.1111/jam.13520.
[49] Braissant O, Bonkat G, Wirz D, Bachmann A. Microbial growth and isothermal microcalorimetry: growth models and their application to microcalorimetric data. Thermochim Acta 2013;555:64–71. https://doi.org/10.1016/j.tca.2012.12.005.
[50] Schaarschmidt B, Lamprecht I. Microcalorimetric study of yeast growth, utilization of different carbohydrates. Thermochim Acta 1978;22:333–8. https://doi.org/10.1016/0040-6031(78)85099-0.
[51] Fan DD, Wang LH, Shang LA, Shi HJ, Ma XX, Mi Y, et al. A microcalorimetric method for studying the biological effects of Mg^{2+} ion on recombinant *Escherichia coli*. Chem Biochem Eng 2008;22:363–8. https://doi.org/10.15255/CABEQ.2014.356.
[52] Francois K, Devlieghere F, Standaert AR, Geeraerd AH, Cools I, Van Impe JF, et al. Environmental factors influencing the relationship between optical density and cell count for *Listeria monocytogenes*. J Appl Microbiol 2005;99:1503–15. https://doi.org/10.1111/j.1365-2672.2005.02727.x.
[53] Sb Pu, Ma Zj, Wang Q. Anti-*Staphylococcus aureus* evaluation of gallic acid by isothermal microcalorimetry and principle component analysis. J Therm Anal Calorim 2019;136:1425–32. https://doi.org/10.1007/s10973-018-7726-5.
[54] Cabadaj M, Bashir S, Haskins D, Said J, McCoubrey L, Gaisford S, et al. Kinetic analysis of microcalorimetric data derived from microbial growth: basic theoretical, practical and industrial considerations. J Microbiol Methods 2021;187:106276. https://doi.org/10.1016/j.mimet.2021.106276.
[55] Trampuz A, Salzmann S, Antheaume J, Daniels AU. Microcalorimetry: a novel method for detection of microbial contamination in platelet products. Transfusion 2007;47:1643–50. https://doi.org/10.1111/j.1537-2995.2007.01336.x.
[56] Baldoni D, Hermann H, Frei R, Trampuz A, Steinhuber A. Performance of microcalorimetry for early detection of methicillin resistance in clinical isolates of *Staphylococcus aureus*. J Clin Microbiol 2009;47:774–6. https://doi.org/10.1128/JCM.02374-08.
[57] von Ah U, Wirz D, Daniels AU. Rapid differentiation of methicillin-susceptible *Staphylococcus aureus* and methicillin-resistant *S. aureus* and MIC determination by isothermal microcalorimetry. J Clin Microbiol 2008;46:2083–7. https://doi.org/10.1128/jcm.00611-08.
[58] Braissant O, Wirz D, Goepfert B, Daniels AU. "The heat is on": rapid microcalorimetric detection of mycobacteria in culture. Tuberculosis 2010;90:57–9. https://doi.org/10.1016/j.tube.2009.11.001.
[59] Borens O, Corvec S, Trampuz A. Diagnosis of periprosthetic joint infections. Hip Int 2012;22(Suppl. 8):S9–14. https://doi.org/10.5301/HIP.2012.9565.
[60] Morgenstern C, Renz N, Cabric S, Perka C, Trampuz A. Multiplex polymerase chain reaction and microcalorimetry in synovial fluid: can pathogen-based detection assays improve the diagnosis of septic arthritis? J Rheumatol 2018;45:1588–93. https://doi.org/10.3899/jrheum.180311.
[61] Morgenstern C, Renz N, Cabric S, Maiolo E, Perka C, Trampuz A. Thermogenic diagnosis of periprosthetic joint infection by microcalorimetry of synovial fluid. BMC Musculoskelet Disord 2020;21:345. https://doi.org/10.1186/s12891-020-03366-3.
[62] Yusuf E, Steinrücken J, Nordback S, Trampuz A. Necrotizing fasciitis after breast augmentation: rapid microbiologic detection by using sonication of removed implants and microcalorimetry. Am J Clin Pathol 2014;142:269–72. https://doi.org/10.1309/AJCPNA1ZKVK7PHUD.
[63] Cichos KH, Spitler CA, Quade JH, Johnson JP, Johnson MD, Ghanem ES. Isothermal microcalorimetry improves the time to diagnosis of fracture-related infection compared with conventional tissue cultures. Clin Orthop Relat Res 2022;480:1463–73. https://doi.org/10.1097/CORR.0000000000002186.
[64] Corcoll F, Pérez-Prieto D, Karbysheva S, Trampuz A, Fariñas O, Monllau JC. Are hamstring grafts a predisposing factor to infection in R-ACL surgery? A comparative in vitro study. Pathogens 2023;12:761. https://doi.org/10.3390/pathogens12060761.
[65] Kuršumovic K, Charalambous CP. Relationship of graft type and vancomycin presoaking to rate of infection in anterior cruciate ligament reconstruction: a meta-analysis of 198 studies with 68,453 grafts. JBJS Rev 2020;8:e1900156. https://doi.org/10.2106/JBJS.RVW.19.00156.
[66] Clauss M, Tafin UF, Bizzini A, Trampuz A, Ilchmann T. Biofilm formation by staphylococci on fresh, fresh-frozen and processed human and bovine bone grafts. Eur Cell Mater 2013;25:159–66. https://doi.org/10.22203/ecm.v025a11.
[67] Bjarnsholt T, Alhede M, Alhede M, Eickhardt-Sørensen SR, Moser C, Kühl M, et al. The in vivo biofilm. Trends Microbiol 2013;21:466–74. https://doi.org/10.1016/j.tim.2013.06.002.
[68] Top Hartmann K, Lund Nielsen R, Mikkelsen FC, Aalbæk B, Lichtenberg M, Holm Jakobsen T, et al. Bacterial micro-aggregates as inoculum in animal models of implant-associated infections. Biofilm 2024;7:100200. https://doi.org/10.1016/j.bioflm.2024.100200.
[69] Heng Z, Congyi Z, Cunxin W, Jibin W, Chaojiang G, Jie L, et al. Microcalorimetric study of virus infection: the effects of hyperthermia and a 1b recombinant homo interferon on the infection process of BHK-21 cells by foot and mouth disease virus. J Therm Anal Calorim 2005;75:45–50. https://doi.org/10.1007/s10973-004-0560-y.
[70] Manneck T, Braissant O, Ellis W, Keiser J. *Schistosoma mansoni*: Antischistosomal activity of the four optical isomers and the two racemates of mefloquine on schistosomula and adult worms in vitro and in vivo. Exp Parasitol 2011;127:260–9. https://doi.org/10.1016/j.exppara.2010.08.011.
[71] Li X, Liu Y, Zhao R, Wu J, Shen X, Qu S. Microcalorimetric study of *Escherichia coli* growth inhibited by the selenomorpholine complexes. Biol Trace Elem Res 2000;75:167–75. https://doi.org/10.1385/BTER:75:1-3:167.
[72] Baldoni D, Steinhuber A, Zimmerli W, Trampuz A. In vitro activity of gallium maltolate against staphylococci in logarithmic, stationary, and biofilm growth phases: comparison of conventional and calorimetric susceptibility testing methods. Antimicrob Agents Chemother 2010;54:157–63. https://doi.org/10.1128/AAC.00700-09.
[73] Yang LN, Xu F, Sun XN, Zhao ZB, Song GC. Microcalorimetric studies on the action of different cephalosporins. J Therm Anal Calorim 2008;93:417–21. https://doi.org/10.1007/s10973-007-8680-9.
[74] Aveledo R, Lago N, Mato MM, Legido JL. Microcalorimetric study of the bactericidal action of titanium tetrachloride on the *Pseudomonas aeruginosa* growth. Potential implications in orthopaedic surgery. Thermochim Acta 2024;739:179807. https://doi.org/10.1016/j.tca.2024.179807.
[75] von Ah U, Wirz D, Daniels AU. Isothermal Micro calorimetry—a new method for MIC determinations: results for 12 antibiotics and reference strains of *E. Coli* and *S. Aureus*. BMC Microbiol 2009;9:106. https://doi.org/10.1186/1471-2180-9-106.
[76] Howell M, Wirz D, Daniels AU, Braissant O. Application of a microcalorimetric method for determining drug susceptibility in Mycobacterium species. J Clin Microbiol 2011;50:16–20. https://doi.org/10.1128/jcm.05556-11.
[77] Huang Y, Ma S, Jing Z. Preparation of Cu (II)/PEI–QPEI/SiO_2 nanopowder as antibacterial material. J Sol-Gel Sci Technol 2014;72:351–8. https://doi.org/10.1007/s10971-014-3439-9.

[78] Thein E, Tafin UF, Betrisey B, Trampuz A, Borens O. In vitro activity of gentamicin-loaded bioabsorbable beads against different microorganisms. Materials 2013;6:3284–93. https://doi.org/10.3390/ma6083284.
[79] Butini ME, Cabric S, Trampuz A, Di Luca M. In vitro anti-biofilm activity of a biphasic gentamicin-loaded calcium sulfate/hydroxyapatite bone graft substitute. Colloids Surf B Biointerfaces 2018;161:252–60. https://doi.org/10.1016/j.colsurfb.2017.10.050.
[80] Gonzalez Moreno M, Butini ME, Maiolo EM, Sessa L, Trampuz A. Antimicrobial activity of bioactive glass S53P4 against representative microorganisms causing osteomyelitis – real-time assessment by isothermal microcalorimetry. Colloids Surf B Biointerfaces 2020;189:110853. https://doi.org/10.1016/j.colsurfb.2020.110853.
[81] Müller N, Kollert M, Trampuz A, Gonzalez Moreno M. Efficacy of different bioactive glass S53P4 formulations in biofilm eradication and the impact of pH and osmotic pressure. Colloids Surf B Biointerfaces 2024;239:113940. https://doi.org/10.1016/j.colsurfb.2024.113940.
[82] von Rege H, Sand W. Evaluation of biocide efficacy by microcalorimetric determination of microbial activity in biofilms. J Microbiol Methods 1998;33:227–35. https://doi.org/10.1016/S0167-7012(98)00055-4.
[83] Astasov-Frauenhoffer M, Braissant O, Hauser-Gerspach I, Daniels AU, Weiger R, Waltimo T. Isothermal microcalorimetry provides new insights into biofilm variability and dynamics. FEMS Microbiol Lett 2012;337:31–7. https://doi.org/10.1111/1574-6968.12007.
[84] Wang L, Di Luca M, Tkhilaishvili T, Trampuz A, Gonzalez Moreno M. Synergistic activity of fosfomycin, ciprofloxacin, and gentamicin against *Escherichia coli* and *Pseudomonas aeruginosa* biofilms. Front Microbiol 2019;10:2522. https://doi.org/10.3389/fmicb.2019.02522.
[85] Solokhina A, Bonkat G, Braissant O. Measuring the metabolic activity of mature mycobacterial biofilms using isothermal microcalorimetry. In: Ennifar E, editor. Microcalorimetry of biological molecules. Methods in molecular biology. vol. 1964. New York, NY: Humana Press; 2019. https://doi.org/10.1007/978-1-4939-9179-2_11.
[86] Zaugg LK, Astasov-Frauenhoffer M, Braissant O, Hauser-Gerspach I, Waltimo T, Zitzmann N. Determinants of biofilm formation and cleanability of titanium surfaces. Clin Oral Implants Res 2017;28:469–75. https://doi.org/10.1111/clr.12821.
[87] Ravn C, Ferreira IS, Maiolo E, Overgaard S, Trampuz A. Microcalorimetric detection of staphylococcal biofilm growth on various prosthetic biomaterials after exposure to daptomycin. J Orthop Res 2018;36:2809–16. https://doi.org/10.1002/jor.24040.
[88] Holeczek H, deWild M, Ruegg J, Gruner P, Moser W, Braissant O. Evaluation of antimicrobial performance of calcium dihydroxide (ca$(OH)_2$) coating on Ti for potential metallic orthopedic implant applications. Antibiotics 2025;14:91. https://doi.org/10.3390/antibiotics14010091.
[89] Braissant O, Chavanne P, de Wild M, Pieles U, Stevanovic S, Schumacher R, et al. Novel microcalorimetric assay for antibacterial activity of implant coatings: the cases of silver-doped hydroxyapatite and calcium hydroxide. J Biomed Mater Res B Appl Biomater 2015;103:1161–7. https://doi.org/10.1002/jbm.b.33294.
[90] Clauss M, Trampuz A, Borens O, Bohner M, Ilchmann T. Biofilm formation on bone grafts and bone graft substitutes: comparison of different materials by a standard in vitro test and microcalorimetry. Acta Biomater 2010;6:3791–7. https://doi.org/10.1016/j.actbio.2010.03.011.
[91] Clauss M, Furustrand Tafin U, Betrisey B, van Garderen N, Trampuz A, Ilchmann T, et al. Influence of physico-chemical material characteristics on staphylococcal biofilm formation- a qualitative and quantitative in vitro analysis of five different calcium phosphate bone grafts. Eur Cell Mater 2014;28:39–50. https://doi.org/10.22203/ecm.v028a04.
[92] Furustrand Tafin U, Betrisey B, Bohner M, Ilchmann T, Trampuz A, Clauss M. Staphylococcal biofilm formation on the surface of three different calcium phosphate bone grafts: a qualitative and quantitative in vivo analysis. J Mater Sci Mater Med 2015;26:130. https://doi.org/10.1007/s10856-015-5467-6.
[93] Czuban M, Wulsten D, Wang L, Di Luca M, Trampuz A. Release of different amphotericin B formulations from PMMA bone cements and their activity against *Candida* biofilm. Colloids Surf B Biointerfaces 2019;183:110406. https://doi.org/10.1016/j.colsurfb.2019.110406.
[94] Farto-Vaamonde X, Diaz-Gomez L, Parga A, Otero A, Concheiro A, Alvarez-Lorenzo C. Perimeter and carvacrol-loading regulate angiogenesis and biofilm growth in 3D printed PLA scaffolds. J Control Release 2022;352:776–92. https://doi.org/10.1016/j.jconrel.2022.10.060.
[95] Virzì NF, Diaz-Rodriguez P, Concheiro A, Otero A, Mazzaglia A, Pittalà V, et al. Combining antibacterial and wound healing features: xanthan gum/guar gum 3D-printed scaffold tuned with hydroxypropyl-β-cyclodextrin/thymol and Zn^{2+}. Carbohydr Polym 2025;351:123069. https://doi.org/10.1016/j.carbpol.2024.123069.
[96] Donaghy C, Javellana G, Hong YJ, Djoko K, Angeles-Boza AM. The synergy between zinc and antimicrobial peptides: an insight into unique bioinorganic interactions. Molecules 2023;28:2156. https://doi.org/10.3390/molecules28052156.
[97] Tkhilaishvili T, Wang L, Tavanti A, Trampuz A, Di Luca M. Antibacterial efficacy of two commercially available bacteriophage formulations, staphylococcal bacteriophage and PYO bacteriophage, against methicillin-resistant *Staphylococcus aureus*: prevention and eradication of biofilm formation and control of a systemic infection of *galleria mellonella* larvae. Front Microbiol 2020;11:110. https://doi.org/10.3389/fmicb.2020.00110.
[98] Fanaei Pirlar R, Wagemans J, Kunisch F, Lavigne R, Trampuz A, Gonzalez Moreno M. Novel *Stenotrophomonas maltophilia* bacteriophage as potential therapeutic agent. Pharmaceutics 2022;14:2216. https://doi.org/10.3390/pharmaceutics14102216.
[99] Fanaei Pirlar R, Wagemans J, Ponce Benavente L, Lavigne R, Trampuz A, Gonzalez Moreno M. Novel bacteriophage specific against *Staphylococcus epidermidis* and with antibiofilm activity. Viruses 2022;14:1340. https://doi.org/10.3390/v14061340.
[100] Chen B, Ponce Benavente L, Chittò M, Wychowaniec JK, Post V, D'Este M, et al. Alginate microbeads and hydrogels delivering meropenem and bacteriophages to treat *Pseudomonas aeruginosa* fracture-related infections. J Control Release 2023;364:159–73. https://doi.org/10.1016/j.jconrel.2023.10.029.
[101] Tkhilaishvili T, Lombardi L, Klatt AB, Trampuz A, Di Luca M. Bacteriophage Sb-1 enhances antibiotic activity against biofilm, degrades exopolysaccharide matrix and targets persisters of *Staphylococcus aureus*. Int J Antimicrob Agents 2018;52:842–53. https://doi.org/10.1016/j.ijantimicag.2018.09.006.
[102] Gonzalez Moreno M, Trampuz A, Di Luca M. Synergistic antibiotic activity against planktonic and biofilm-embedded *Streptococcus agalactiae*, *Streptococcus pyogenes* and *Streptococcus oralis*. J Antimicrob Chemother 2017;72:3085–92. https://doi.org/10.1093/jac/dkx265.
[103] Yilmaz C, Colak M, Yilmaz BC, Ersoz G, Kutateladze M, Gozlugol M. Bacteriophage therapy in implant-related infections: an experimental study. J Bone Joint Surg Am 2013;95:117–25. https://doi.org/10.2106/JBJS.K.01135.
[104] Wang L, Tkhilaishvili T, Trampuz A, Gonzalez Moreno M. Evaluation of staphylococcal bacteriophage Sb-1 as an adjunctive agent to antibiotics against rifampin-resistant *Staphylococcus aureus* biofilms. Front Microbiol 2020;11:602057. https://doi.org/10.3389/fmicb.2020.602057.
[105] Butini ME, Abbandonato G, Di Rienzo C, Trampuz A, Di Luca M. Isothermal microcalorimetry detects the presence of persister cells in a *Staphylococcus aureus* biofilm after vancomycin treatment. Front Microbiol 2019;10:332. https://doi.org/10.3389/fmicb.2019.00332.
[106] Scheper H, Wubbolts JM, Verhagen JAM, de Visser AW, van der Wal RJP, Visser LG, et al. SAAP-148 eradicates MRSA Persisters within mature biofilm models simulating prosthetic joint infection. Front Microbiol 2021;12:625952. https://doi.org/10.3389/fmicb.2021.625952.
[107] Karbysheva S, Di Luca M, Butini ME, Winkler T, Schütz M, Trampuz A. Comparison of sonication with chemical biofilm dislodgement methods using chelating and reducing agents: implications for the microbiological diagnosis of implant associated infection. PloS One 2020;15:e0231389. https://doi.org/10.1371/journal.pone.0231389.
[108] Beezer AE, Gaisford S, Hills AK, Willson RJ, Mitchell JC. Pharmaceutical microcalorimetry: applications to long-term stability studies. Int J Pharm 1999;179:159–65. https://doi.org/10.1016/s0378-5173(98)00336-6.
[109] Lewis G, Daniels AU. Use of isothermal heat-conduction microcalorimetry (IHCMC) for the evaluation of synthetic biomaterials. J Biomed Mater Res B Appl Biomater 2003;66:487–501. https://doi.org/10.1002/jbm.b.10044.
[110] Gaisford S. Stability assessment of pharmaceuticals and biopharmaceuticals by isothermal calorimetry. Curr Pharm Biotechnol 2005;6:181–91. https://doi.org/10.2174/1389201054022913.
[111] Charlebois SJ, Daniels AU, Lewis G. Isothermal microcalorimetry: An analytical technique for assessing the dynamic chemical stability of UHMWPE. Biomaterials 2003;24:291–6. https://doi.org/10.1016/S0142-9612(02)00317-4.
[112] Hardison A, Lewis G, Daniels AU, Smith RA. Determination of the activation energies of and aggregate rates for exothermic physico-chemical changes in UHMWPE by isothermal heat-conduction microcalorimetry (IHCMC). Biomaterials 2003;24:5145–51. https://doi.org/10.1016/s0142-9612(03)00461-7.
[113] Daniels AU, Wirz D, Morscher E. The well-cemented total-hip arthroplasty. Breusch, S., Malchau, H., Eds. Heidelberg, Germany: Springer; 2005. p. 381.
[114] Lewis G, Son Y. Thermal stability of acrylic bone cement powder under shelf storage conditions: an isothermal microcalorimetric study. Biomed Mater Eng 2018;18:83–90. https://doi.org/10.3233/BME-2008-0511.
[115] Wadsö I. Applications of an eight-channel isothermal conduction calorimeter for cement hydration studies. Cem Int 2005;1:94–101.
[116] Hofelich TA, Wadsö L, Smith AL, Shirazi H, Mulligan RS. The isothermal heat conduction calorimeter: a versatile instrument for studying processes in physics, chemistry, and biology. J Chem Educ 2001;78:1080–6. https://doi.org/10.1021/ed078p1080.
[117] Wang Y, Zhu H, Feng J, Neuzil P. Recent advances of microcalorimetry for studying cellular metabolic heat. TrAC-Trends Anal Chem 2021;143:116353. https://doi.org/10.1016/j.trac.2021.116353.
[118] Boettcher H, Nittinger J, Engel S, Furst P. Thermogenesis of white adipocytes: a novel method allowing long-term microcalorimetric investigations. J Biochem Biophys Methods 1991;23:181–7. https://doi.org/10.1016/0165-022X(91)90065-5.
[119] Boettcher H, Engel S, Furst P. Thermogenesis and metabolism of human white adipocytes in gel culture. Clin Nutr 1992;11:53–5. https://doi.org/10.1016/0261-5614(92)90065-X.
[120] Bataillard P. Calorimetric sensing in bioanalytical chemistry: principles, applications and trends. TrAC-Trends Anal Chem 1993;12:387–94. https://doi.org/10.1016/0165-9936(93)80002-2.
[121] Soerbis R, Monti M, Nilsson-Ehle P, Wadsö I. Heat production by adipocytes from obese subjects before and after weight reduction. Metabolism 1982;31:973–9. https://doi.org/10.1016/0026-0495(82)90137-8.
[122] West GB, Woodruff WH, Brown JH. Allometric scaling of metabolic rate from molecules and mitochondria to cells and mammals. PNAS 2002;99:2473–8. https://doi.org/10.1073/pnas.012579799.

[123] Fagher B, Liedholm H, Monti M, Moritz U. Thermogenesis in human skeletal muscle as measured by direct microcalorimetry and muscle contractile performance during beta-adrenoceptor blockade. Clin Sci (Lond) 1986;70:435–41. https://doi.org/10.1042/cs0700435.
[124] Fagher B, Liedholm H, Sjogren A, Monti M. Effects of terbutaline on basal thermogenesis of human skeletal muscle and Na-K pump after 1 week of oral use—a placebo controlled comparison with propranolol. Br J Clin Pharmacol 1993;35:629–35. https://doi.org/10.1111/j.1365-2125.1993.tb04193.x.
[125] Fagher B, Monti M. Thermogenic effect of two p-adrenoceptor blocking drugs, propranolol and carvedilol, on skeletal muscle in rats. A microcalorimetric study. Thermochim Acta 1995;251:183–9. https://doi.org/10.1016/0040-6031(94)02010-L.
[126] Kallerhoff M, Karnebogen M, Singer D, Dettenbaeh A, Gralher U, Ringert RH. Microcalorimetric measurements carried out on isolated tumorous and nontumorous tissue samples from organs in the urogenital tract in comparison to histological and impulse-cytophotometric investigations. Urol Res 1996;24:83–91. https://doi.org/10.1007/BF00431084.
[127] Sung HW, Chen WY, Tsai CC, Hsu HL. In vitro study of enzymatic degradation of biological tissues fixed by glutaraldehyde or epoxy compound. J Biomater Sci Polym Ed 1997;8:587–600. https://doi.org/10.1163/156856297x00191.
[128] Kemp RB, Guan YH. The application of heat flux measurements to improve the growth of mammalian cells in culture. Thermochim Acta 2000;349:23–30. https://doi.org/10.1016/S0040-6031(99)00493-1.
[129] Kemp RB. The application of heat conduction microcalorimetry to study the metabolism and pharmaceutical modulation of cultured mammalian cells. Thermochim Acta 2001;380:229–44. https://doi.org/10.1016/S0040-6031(01)00676-1.
[130] Santoro R, Braissant O, Müller B, Wirz D, Daniels AU, Martin I, et al. Real-time measurements of human chondrocyte heat production during in vitro proliferation. Biotechnol Bioeng 2011;108:3019–24. https://doi.org/10.1002/bit.23268.
[131] Ma J, Qi WT, Yang LN, Yu WT, Xie YB, Wang W, et al. Microcalorimetric study on the growth and metabolism of microencapsulated microbial cell culture. J Microbiol Methods 2007;68:172–7. https://doi.org/10.1016/j.mimet.2006.07.007.
[132] Xie Y, DePierre JW, Nässberger L. Biocompatibility of microplates for culturing epithelial renal cells evaluated by a microcalorimetric technique. J Mater Sci Mater Med 2000;11:587–91. https://doi.org/10.1023/A:1008984304821.
[133] Monti M, Ikomi-Kumm J, Ljunggren L, Lund U, Thysell H. Medical application of microcalorimetry in human toxicology. A study of blood compatibility of hemodialysis membranes. Pure Appl Chem 1993;65(9):1979–81. https://doi.org/10.1351/pac199365091979.
[134] Liu W, Chaspoul F, Berge Lefranc D, Decome L, Gallice P. Microcalorimetry as a tool for Cr(VI) toxicity evaluation of human dermal fibroblasts. J Therm Anal Calorim 2007;89:21–4. https://doi.org/10.1007/s10973-006-7918-2.
[135] Belliardo C, Gallice P, Chaspoul F, Corréard F, Bergé-Lefranc D. Effect of Ni(II), Cd (II) and Al(III) on human fibroblast bioenergetics, a preliminary comparative study. J Therm Anal Calorim 2016;123:2543–7. https://doi.org/10.1007/s10973-016-5289-x.
[136] Nässberger L, Monti M. Effect of gentamicin on human blood cells metabolism as measured by microcalorimetry. Hum Toxicol 1987;6(3):223–6. https://doi.org/10.1177/096032718700600309.
[137] Doostmohammadi A, Monshi A, Fathi MH, Karbasi S, Braissant O, Daniels AU. Direct cytotoxicity evaluation of 63S bioactive glass and bone-derived hydroxyapatite particles using yeast model and human chondrocyte cells by microcalorimetry. J Mater Sci Mater Med 2011;22:2293. https://doi.org/10.1007/s10856-011-4400-x.
[138] Charlebois SJ, Daniels AU, Smith RA. Metabolic heat production as a measure of macrophage response to particles from orthopedic implant materials. J Biomed Mater Res 2002;59:166–75. https://doi.org/10.1002/jbm.1230.
[139] Wang T, Zhou X, Zou W, Zhang P, Wang J, Li H, et al. Synergistic effects of Ginseng C. A. Mey and Astragalus membranaceus (Fisch.) Bunge on activating mice splenic lymphocytes detected by microcalorimetry and the underlying mechanisms predicted by in silico network analysis. J Therm Anal Calorim 2018;132:1933–42. https://doi.org/10.1007/s10973-018-7109-y.
[140] Monti M. In vitro thermal studies of blood cells. In: James MA, editor. Thermal and energetic studies of cellular biological systems. Wright, Bristol; 1987. p. 131–46.
[141] Swartbol P, Pärsson H, Nässberger L, Norgren L. Metabolic response of blood cells to synthetic graft-materials with special reference to a fluoromer passivated Dacron graft. An in vitro study using microcalorimetry. Int J Artif Organs 1995;18:372–9. https://doi.org/10.1002/jbm.820290412.
[142] Pärsson H, Nässberger L, Thörne J, Norgren L. Metabolic response of granulocytes and platelets to synthetic vascular grafts: preliminary results with an in vitro technique. J Biomed Mater Res 1995;29:519–25. https://doi.org/10.1002/jbm.820290412.
[143] An-Min T, Chang-Li X, Song-Chen Q, Ping K, Yu G. Microcalorimetric study of mitochondria isolated from fish liver tissue. J Biochem Biophys Methods 1996;31:189–93. https://doi.org/10.1016/0165-022x(95)00034-o.
[144] Deng FJ, Li FJ, Liu Y, Liu YW, Wang CX, Liu SY, et al. Microcalorimetric studies on the mitochondria metabolism of *Cyprinus Carpio* val and its parents. Chin J Chem 2001;19:1023–7. https://doi.org/10.1002/cjoc.20010191103.
[145] Zhao J, Ma L, Xiang X, Guo QL, Jiang FL, Liu Y. Microcalorimetric studies on the energy release of isolated rat mitochondria under different concentrations of gadolinium (III). Chemosphere 2016;153:414–8. https://doi.org/10.1016/j.chemosphere.2016.03.082.
[146] Monti M, Brandt L, Ikomi-Kumm J, Losson H. Heat production rate in blood lymphocytes as a prognostic factor in non-Hodgkin's lymphoma. Eur J Haematol 1990;4:250–4. https://doi.org/10.1111/j.1600-0609.1990.tb00469.x.
[147] Kallerhoff M, Karnebogen M, Singer D, Dettenbaeh A, Gralher U, Ringert RH. Microcalorimetric measurements carried out on isolated tumorous and nontumorous tissue samples from organs in the urogenital tract in comparison to histological and impulse-cytophotometric investigations. Urol Res 1996;24:83–91. https://doi.org/10.1007/BF00431084.
[148] Moreno-Sanchez R, Hernández-Marin A, Saavedra E, Pardo JP, Ralph SJ, Rodriguez-Enriquez S. Who controls the ATP supply in cancer cells? Biochemistry lessons to understand cancer energy metabolism. Int J Biochem Cell Biol 2014;50:10–23. https://doi.org/10.1016/j.biocel.2014.01.025.
[149] Lemos D, Oliveira T, Martins L, de Azevedo VR, Rodrigues MF, Ketzer LA, et al. Isothermal microcalorimetry of tumor cells: enhanced thermogenesis by metastatic cells. Front Oncol 2019;9:1430. https://doi.org/10.3389/fonc.2019.01430.
[150] Braissant O, Keiser J, Meister I, Bachmann A, Wirz D, Göpfert B, et al. Isothermal microcalorimetry accurately detects bacteria, tumorous microtissues, and parasitic worms in a label-free well-plate assay. Biotechnol J 2015;10:460–8. https://doi.org/10.1002/biot.201400494.
[151] Pereira da Silva CM, Pedroso de Lima MC. Application of flow microcalorimetry to the study of dehydrofolate reductase activities in crude tissue homogenates. J Thermal Anal 1992;38:821–33. https://doi.org/10.1007/BF01979414.
[152] Gros SJ, Holland-Cunz SG, Supuran CT, Braissant O. Personalized treatment response assessment for rare childhood tumors using microcalorimetry-exemplified by use of carbonic anhydrase IX and aquaporin 1 inhibitors. Int J Mol Sci 2019;20:4984. https://doi.org/10.3390/ijms20204984.
[153] Huo Z, Bilang R, Supuran CT, von derWeid N, Bruder E, Holland-Cunz S, et al. Perfusion-based bioreactor culture and isothermal microcalorimetry for preclinical drug testing with the carbonic anhydrase inhibitor SLC-0111 in patient-derived neuroblastoma. Int J Mol Sci 2022;23:3128. https://doi.org/10.3390/ijms23063128.
[154] Ting NL, Lau HC, Yu J. Cancer pharmacomicrobiomics: targeting microbiota to optimise cancer therapy outcomes. Gut 2022;71:1412–25. https://doi.org/10.1136/gutjnl-2021-326264.
[155] Khan AA, Sirsat AT, Singh H, Cash P. Microbiota and cancer: current understanding and mechanistic implications. Clin Transl Oncol 2022;24:193–202. https://doi.org/10.1007/s12094-021-02690-x.
[156] Guo X, Wang P, Li Y, Chang Y, Wang X. Microbiomes in pancreatic cancer can be an accomplice or a weapon. Crit Rev Oncol Hematol 2024;194:104262. https://doi.org/10.1016/j.critrevonc.2024.104262.
[157] Panebianco C, Adamberg K, Adamberg S, Saracino C, Jaagura M, Kolk K, et al. Engineered resistant-starch (ERS) diet shapes colon microbiota profile in parallel with the retardation of tumor growth in in vitro and in vivo pancreatic cancer models. Nutrients 2017;27:331. https://doi.org/10.3390/nu9040331.
[158] Pini N, Huo Z, Holland-Cunz S, Gros SJ. Increased proliferation of neuroblastoma cells under fructose metabolism can be measured by isothermal microcalorimetry. Children 2021;8:784. https://doi.org/10.3390/children8090784.
[159] Li L, Tian YC, Tadé MO, Feng Y, Qu SS. Apoptosis of tumour cells by temperature and anti-tumour drug: microscopic and macroscopic investigations. J Therm Biol 2003;28:321–9. https://doi.org/10.1016/S0306-4565(03)00008-1.
[160] Hernández Garcia A, Herrmann AM, Håkansson S. Isothermal microcalorimetry for rapid viability assessment of freeze-dried *Lactobacillus reuteri*. Process Biochem 2017;55:49–54. https://doi.org/10.1016/j.procbio.2017.01.012.
[161] Yoon S, Lim MH, Park SC, Shin JS, Kim YJ. *Neisseria meningitidis* detection based on a microcalorimetric biosensor with a split-flow microchannel. J Microelectromech Syst 2008;17:590–8. https://doi.org/10.1109/JMEMS.2008.924846.
[162] Vehusheia SLK, Roman CI, Arnoldini M, Hierold C. Experimental in vitro microfluidic calorimetric chip data towards the early detection of infection on implant surfaces. Sensors 2024;24:1019. https://doi.org/10.3390/s24031019.
[163] Zhu H, Wang L, Feng J, Neuzil P. The development of ultrasensitive microcalorimeters for bioanalysis and energy balance monitoring. Fundamental Res 2024;4:1625–38. https://doi.org/10.1016/j.fmre.2023.01.011.
[164] Bokhari MH, Halleskog C, Åslund A, Boulet N, Casadesús Rendos E, de Jong JMA, et al. Isothermal microcalorimetry measures UCP1-mediated thermogenesis in mature brite adipocytes. Commun Biol 2021;4:1108. https://doi.org/10.1038/s42003-021-02639-4.
[165] Myers E, Brahmachary P, Mensah S, Putnam C, Carlson RP, Greenwood M, et al. Chondrocytes embedded in agarose generate distinct metabolic heat profiles based on media carbon sources. Ann Biomed Eng 2025. https://doi.org/10.1007/s10439-025-03755-6. in press.
[166] Cichos KH, Christie MC, Ponce BA, Ghanem ES. Biofilm growth on orthopaedic cerclage materials: nonmetallic polymers are less resistant to methicillin-resistant *Staphylococcus aureus* bacterial adhesion. J Arthroplasty 2024;39:S469–75. https://doi.org/10.1016/j.arth.2024.04.042.
[167] Oudebrouckx G, Goossens J, Bormans S, Vandenryt T, Wagner P, Thoelen R. Integrating thermal sensors in a microplate format: simultaneous real-time quantification of cell number and metabolic activity. ACS Appl Mater Interfaces 2022;14:2440–51. https://doi.org/10.1021/acsami.1c14668.
[168] Goossens J, Oudebrouckx G, Vandenryt T, Thoelen R. Microplate-based impedance and thermal sensing system for concurrent cell viability and counting analysis. Talanta 2025;295:128193. https://doi.org/10.1016/j.talanta.2025.128193.

[169] Ikomi-Kumm J, Ljunggren L, Monti M. Thermochemical studies of surface-induced activation in human granulocytes in vitro. J Mater Sci Mater Med 1992;3:151–3. https://doi.org/10.1007/BF00705284.
[170] Laranjeiro R, Harinath G, Burke D, Braeckman BP, Driscoll M. Single swim sessions in *C. elegans* induce key features of mammalian exercise. BMC Biol 2017;15:30. https://doi.org/10.1186/s12915-017-0368-4.
[171] González-Llera L, Arana AJ, Sánchez L, Alvarez-Lorenzo C, Barreiro-Iglesias A. Isothermal calorimetry reveals that successful regeneration after a spinal cord injury in larval zebrafish is associated with an increase in energy expenditure. Biochim Biophys Acta (BBA) Bioenergetics 2024;1865:149498. https://doi.org/10.1016/j.bbabio.2024.149498.
[172] S.5002. To allow for alternatives to animal testing for purposes of drug and biological product applications.. https://www.congress.gov/117/bills/s5002/BILLS-117s5002cps.pdf.
[173] To amend the Federal Food, Drug, and Cosmetic Act to establish a process for the qualification of nonclinical testing methods to reduce and replace the use of animals in nonclinical research, improve the predictivity of nonclinical testing methods, and reduce development time for a biological product or other drug, and for other purposes https://www.govinfo.gov/content/pkg/BILLS-118hr7248ih/pdf/BILLS-118hr7248ih.pdf.